Eur. Phys. J. C 51, 989–1008 (2007)
DOI 10.1140/epjc/s10052-007-0364-x

THE EUROPEAN PHYSICAL JOURNAL C

Special Article – Tools for Experiment and Theory

Simulation of beyond standard model physics in Herwig++

M. Gigg[a], P. Richardson[b]

Institute for Particle Physics Phenomenology, Ogden Centre for Fundamental Physics, Department of Physics, University of Durham, South Rd., Durham DH1 3LE, UK

Received: 2 May 2007 / Revised version: 19 June 2007 /
Published online: 25 July 2007 –

Abstract. We present a new approach for the simulation of beyond standard model (BSM) physics within the Herwig++ event generator. Our approach is more generic than previous methods with the aim of minimising the effort of implementing further new physics models. Spin correlations, which are important for BSM models due to new heavy fermions and bosons, are discussed and their effects demonstrated for the minimal supersymmetric standard model (MSSM) and Randall–Sundrum model using our new framework.

1 Introduction

In the arena of modern particle physics Monte Carlo event generators have become essential tools for analysing experimental data. They are necessary in order to compare the behaviour of theoretical predictions under the conditions present within a collider experiment by giving a realistic description of the final state particles that interact with the detector including any experimental cuts. It is essential that these generators reproduce standard model physics as accurately as possible, since these processes will provide a background to any new physics signals that might be present at future colliders as well as being of interest in their own right. New physics models will also need to be incorporated into a Monte Carlo simulation in order for their implications to be fully understood.

There are a wide variety of new physics models and while one could implement each model independently in its own event generator it is more efficient to have a general purpose event generator that can handle a variety of these models but can also offer the full event simulation framework, i.e. hard process, decay, parton shower and hadronisation. This is the approach that will be described in this paper using the Herwig++ [1, 2] event generator.

Herwig++ is a new event generator, written in C++, based on the well tested HERWIG [3–5] program. It is not simply a translation of the old FORTRAN code into C++; it includes significant improvements to both the physics models and the simulation framework. The object oriented aspect of the C++ language will allow future additions and modifications to be incorporated more easily. One area where improvements are needed is in the simulation of beyond standard model (BSM) physics. In the past each model was hard coded in the generator making the addition of new models a time consuming process. We wish to minimise the effort required in order to add new physics models to Herwig++. Our approach is to factorise the problem into smaller pieces and reuse as much information that has already been calculated as possible.

For example, in gluino production our method would first calculate the $2 \to 2$ production matrix element and then choose a decay mode for the gluino based on the branching ratios and generate the decay products. In addition, since the gluino is a coloured object, there will be QCD radiation, which is simulated more easily in our factorised approach, as it is simply another step between the production and decay of the particle. While factorising the problem in this manner makes many things easier, it does introduce complications when considering spin correlations. Additional information must be passed between each step to ensure that the final decay products are correctly distributed including correlations between the production and various decays.

Other packages, such as MadGraph [6], CompHEP [7], Sherpa [8] and Omega [9] with WHiZard [10] exist, which are capable of producing a wide class of BSM physics processes[1] but they have limitations. The main problem is the efficiency with which the variety of possible processes can be generated. The above programs all treat the processes as $2 \to n$ scattering which requires the exact production and decay chain to be specified from the beginning. While this does mean that effects such as spin correlations are included automatically, it limits the number of processes that can be generated in a reasonable amount of time. For example, in order to study two different decay modes of the gluino, with the above generators, one would have to calculate the production step twice, whereas our

[a] e-mail: m.a.gigg@durham.ac.uk
[b] e-mail: peter.richardson@durham.ac.uk

[1] A general list of programs for BSM physics can be found at http://www.ippp.dur.ac.uk/montecarlo/BSM/

method would simply be able to pick another decay mode without recalculating the hard subprocess.

To minimise the amount of work needed for every new model, our approach will require only a set of Feynman rules, the specification of any new non-standard model particles and their properties. In addition there is a mechanism to read in parameters from a Les Houches [11][2] file for a supersymmetric (SUSY) model. The new physics models currently implemented are the minimal supersymmetric standard model (MSSM) with CP, R-parity and flavour conservation and a Randall–Sundrum [12] type model with the lowest Kaluza–Klein excitation coupling to standard model matter.

Section 2 introduces how spin correlations are dealt with, since these will be important when dealing with heavy fermions and vector bosons. Some details on the technical structure of the code will be given in Sect. 3 along with some physics of the models implemented thus far. A comparison with the FORTRAN code for some physical distributions will be presented in Sect. 4 to demonstrate the consistency of our approach.

2 Spin correlations

Many new physics models predict the existence of new particles that are as yet undetected by experiment. Heavy spin-$\frac{1}{2}$, spin-1 and spin-2 particles will be produced, which will decay to lighter states. Their non-zero spin gives correlations between the production and decay steps that must be taken into account in order for the final state angular distributions to be correct. An algorithm for dealing with these correlations is demonstrated in [13–15]. It will briefly be described below for the process $e^+e^- \to t\bar{t}$, where the top quark subsequently decays, via a W boson, to a b quark and a pair of light fermions.

Initially the outgoing momenta are generated according to the usual cross-section integral,

$$\frac{(2\pi)^4}{2s}\int \frac{\mathrm{d}^3 p_t}{(2\pi)^3 2E_t}\frac{\mathrm{d}^3 p_{\bar{t}}}{(2\pi)^3 2E_{\bar{t}}}\mathcal{M}^{e^+e^-\to t\bar{t}}_{\lambda_t\lambda_{\bar{t}}}\mathcal{M}^{*e^+e^-\to t\bar{t}}_{\lambda_t\lambda_{\bar{t}}}, \tag{1}$$

where $\mathcal{M}^{e^+e^-\to t\bar{t}}_{\lambda_t\lambda_{\bar{t}}}$ is the matrix element for the initial hard process and $\lambda_{t,\bar{t}}$ are the helicity of the t and $\bar{t}$, respectively. One of the outgoing particles is then picked at random, say the top, and a spin density matrix calculated

$$\rho^t_{\lambda_t\lambda_t'} = \frac{1}{N}\mathcal{M}^{e^+e^-\to t\bar{t}}_{\lambda_t\lambda_{\bar{t}}}\mathcal{M}^{*e^+e^-\to t\bar{t}}_{\lambda_t'\lambda_{\bar{t}}}, \tag{2}$$

with N defined such that $\mathrm{Tr}\rho = 1$.

The top is decayed and the momenta of the decay products distributed according to

$$\frac{(2\pi)^4}{2m_t}\int \frac{\mathrm{d}^3 p_b}{(2\pi)^3 2E_b}\frac{\mathrm{d}^3 p_{W^+}}{(2\pi)^3 2E_{W^+}}\rho^t_{\lambda_t\lambda_t'}\mathcal{M}^{t\to bW^+}_{\lambda_t\lambda_{W^+}}\mathcal{M}^{*t\to bW^+}_{\lambda_t'\lambda_{W^+}}, \tag{3}$$

where the inclusion of the spin density matrix ensures the correct correlation between the top decay products and the beam.

A spin density matrix for the W^+ is calculated because the b is stable,

$$\rho^{W^+}_{\lambda_{W^+}\lambda'_{W^+}} = \frac{1}{N}\rho^t_{\lambda_t\lambda_t'}\mathcal{M}^{t\to bW^+}_{\lambda_t\lambda_{W^+}}\mathcal{M}^{*t\to bW^+}_{\lambda_t'\lambda'_{W^+}}, \tag{4}$$

and the W decayed in the same manner as the top with the inclusion of the spin density matrix, here ensuring the correct correlations between the W decay products, the beam and the bottom quark.

The decay products of the W are stable fermions so the decay chain terminates here and a decay matrix for the W,

$$D^{W^+}_{\lambda_{W^+}\lambda'_{W^+}} = \frac{1}{N}\mathcal{M}^{t\to bW^+}_{\lambda_t\lambda_{W^+}}\mathcal{M}^{*t\to bW^+}_{\lambda_t\lambda'_{W^+}}, \tag{5}$$

is calculated. Moving back up the chain, a decay matrix for the top quark is calculated using the decay matrix of the W,

$$D^t_{\lambda_t\lambda_t'} = \frac{1}{N}\mathcal{M}^{t\to bW^+}_{\lambda_t\lambda_{W^+}}\mathcal{M}^{*t\to bW^+}_{\lambda_t'\lambda'_{W^+}}D^{W^+}_{\lambda_{W^+}\lambda'_{W^+}}. \tag{6}$$

Since the top came from the hard subprocess we must now deal with the $\bar{t}$ in a similar manner, but instead of using $\delta_{\lambda_i\lambda_i}$ when calculating the initial spin density matrix, the decay matrix of the top is used and the $\bar{t}$ decay is generated accordingly. The density matrices pass information from one decay chain to the associated chain, thereby preserving the correct correlations.

The production and decay of the top, using the spin correlation algorithm, is demonstrated in Figs. 1–3. The hard subprocess and subsequent decays were generated using our new method. The results from the full matrix element calculation are also included to show that the algorithm has been correctly implemented. The separate plots illustrate the different stages of the algorithm at work. Figure 1 gives the angle between the beam and the outgoing lepton. The results from the simulation agree well with the full matrix element calculation, which demonstrates the consistency of the algorithm for the decay of the $\bar{t}$.

Figure 2 gives the angle between the top quark and the produced lepton. This shows the same agreement as the previous figure and demonstrates the correct implementation of the spin density matrix for the $\bar{t}$ decay. Finally, Fig. 3 gives the results for the angle between the final state lepton/antilepton pair showing the correct implementation of the decay matrix that encodes the information about the $\bar{t}$ decay. Again there is good agreement between our numerical results and the full matrix element calculation giving us confidence about the implementation of the spin correlation algorithm.

The above procedure is well suited for implementation in an event generator, as demonstrated, where one would like additional processes to occur between the hard production and decay such as showering of a coloured particle. The algorithm as presented here is implemented in Herwig++ and will be used extensively during the simulation of many BSM physics models.

[2] Currently only SLHA1 is supported.

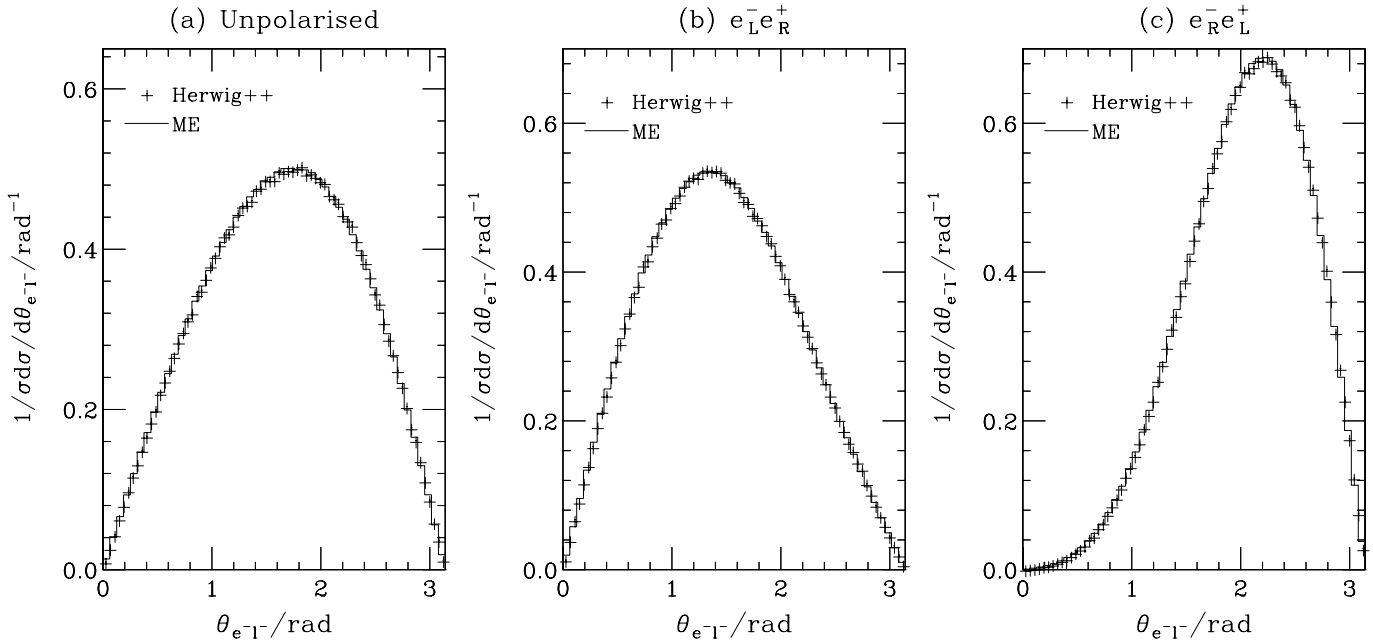

Fig. 1. Angle between the beam and the outgoing lepton in $e^+e^- \to t\bar{t} \to b\bar{b}l^+\nu_l l^-\bar{\nu}_l$ in the lab frame for a centre-of-mass energy of 500 GeV with **a** unpolarised incoming beams, **b** negatively polarised electrons and positively polarised positrons and **c** positively polarised electrons and negatively polarised electrons

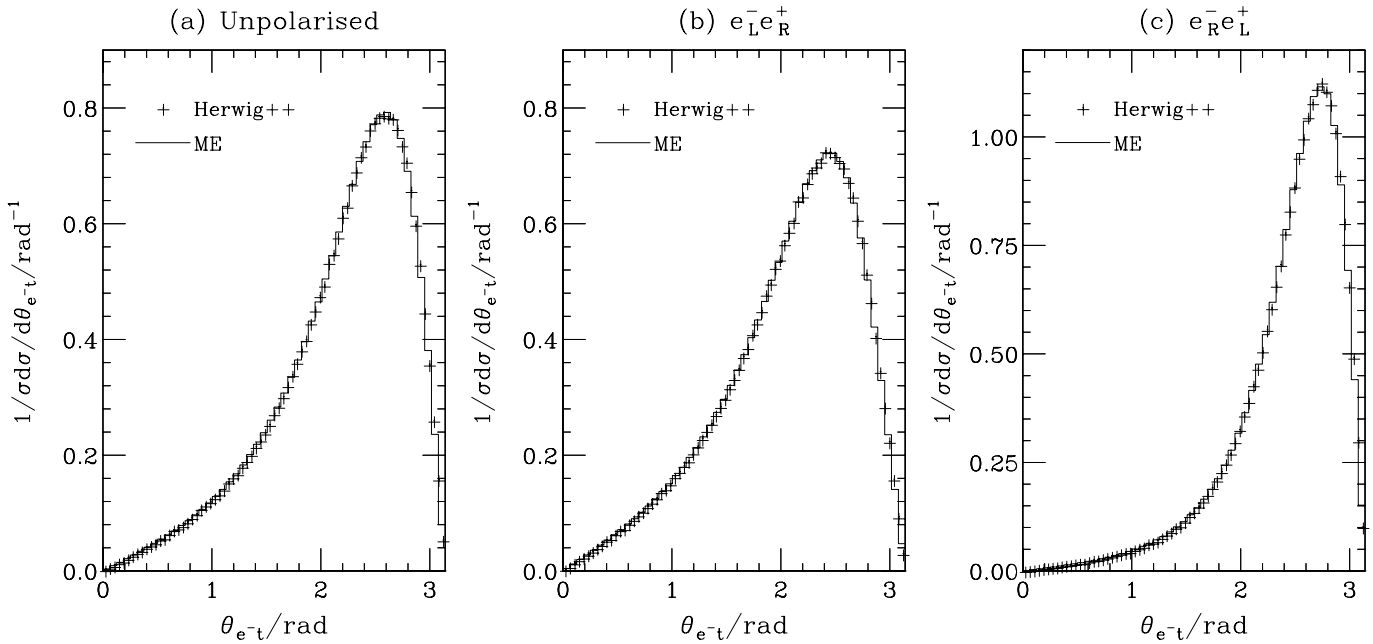

Fig. 2. Angle between the lepton and the top quark in $e^+e^- \to t\bar{t} \to b\bar{b}l^+\nu_l l^-\bar{\nu}_l$ in the lab frame for a centre-of-mass energy of 500 GeV with **a** unpolarised incoming beams, **b** negatively polarised electrons and positively polarised positrons and **c** positively polarised electrons and negatively polarised electrons

3 Technical details

Instead of following the paradigm of implementing a specific model we have chosen a more generic approach to the problem, which is intended to be as model independent as possible. This will allow a wider variety of models to be implemented within the event generator framework. The structure of the code relies heavily on the inheritance facilities available in the C++ language which allow independent structures to have a common heritage.

Due to the existing structure it was sufficient only to consider generation of the hard subprocess and decay of the subsequent unstable particles since the showering and hadronising are handled (almost) independently

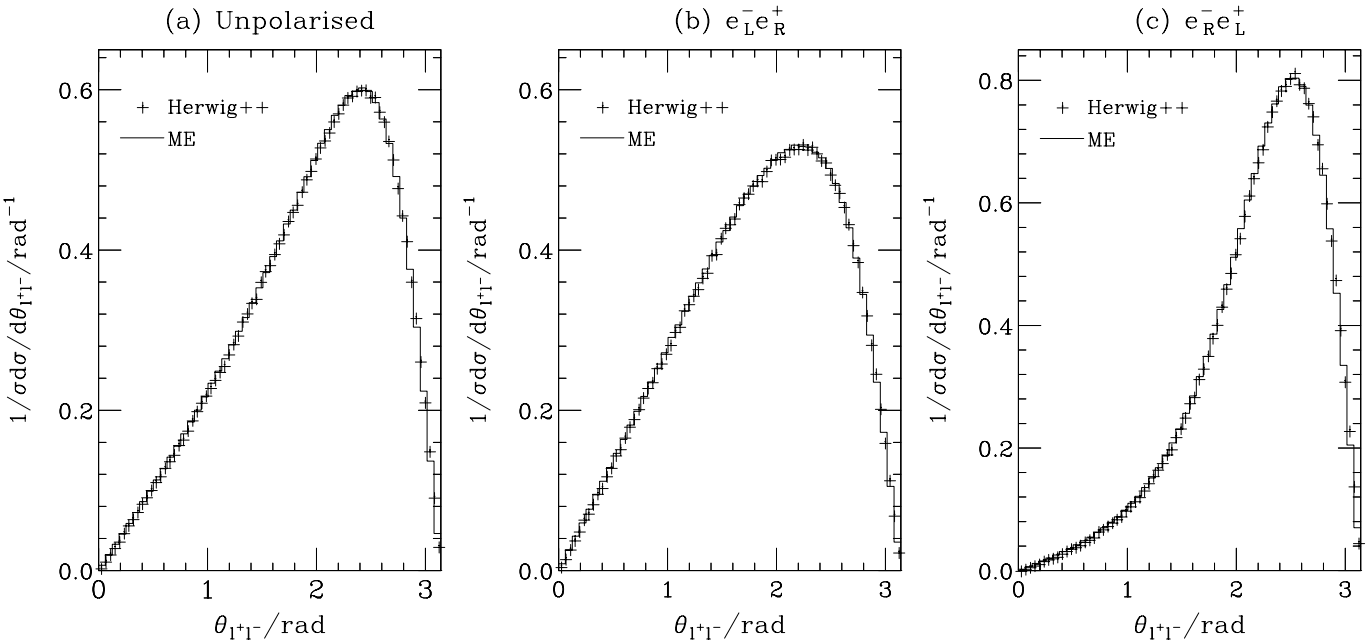

Fig. 3. Angle between the outgoing lepton and anti-lepton in $e^+e^- \to t\bar{t} \to b\bar{b}l^+\nu_l l^-\bar{\nu}_l$ in the lab frame for a centre-of-mass energy of 500 GeV with **a** unpolarised incoming beams, **b** negatively polarised electrons and positively polarised positrons and **c** positively polarised electrons and negatively polarised electrons

of the model details. Both the hard process and decay require knowledge of the Feynman rules, couplings and masses within the model, and these are currently implemented for the MSSM and Randall–Sundrum model.

In Herwig++ the Feynman rules are encoded in Vertex classes. They form part of the structure that enables the calculation of matrix elements using the HELAS formalism [16]. These classes provide the couplings to the particles defined within the model, and so they must be provided with every new model that is implemented. The way in which the vertices have been set up minimises this effort and will be described in the next section.

3.1 Vertices

For a given combination of spins interacting at a vertex, if we assume the perturbative form of the interaction, there is a specific Lorentz structure and a limit on the number of possible couplings for any given interaction. This is carried into the implementation of the vertices by defining a base class that holds all common functionality and by inheriting from this class to define a specific spin structure. The spin structure must then be further specialised into the exact vertex required by specifying the coupling and the particles that are able to interact at it.

As an example, consider the $\chi_i^0\chi_j^0 Z^0$ vertex in the MSSM as shown in Fig. 4.

A more general rule than that given in the figure is

$$\mathrm{i}c\gamma^\mu\left[\frac{a^\mathrm{L}}{2}(1-\gamma_5)+\frac{a^\mathrm{R}}{2}(1+\gamma_5)\right], \qquad (7)$$

where c is the overall normalisation and $a^{\{\mathrm{L,R}\}}$ are the left and right couplings, respectively. We would choose $c = g/\cos\theta_\mathrm{W}$, $a^\mathrm{L} = O'^\mathrm{L}_{ij}$ and $a^\mathrm{R} = O'^\mathrm{R}_{ij}$. The overall coupling c is stored in the base class and the inherited class for the specific spin stores the left and right couplings, since they may not always be required. Finally, the actual vertex class implements a function to calculate the value of the couplings.

In addition to storing the couplings, the spin specific vertices have functions that can be used to either evaluate the vertex as a complex number or return an appropriate off-shell wave function. The ability to calculate not just the entire vertex but off-shell components underlies the HELAS [16] formalism for the calculation of matrix elements. As an example consider decay of the top as in Sect. 2. The HELAS approach factorises the problem into two parts. First a vector wave function for an off-shell W^+ is calculated for a specified helicity of the top and bottom

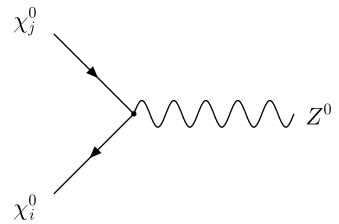

$$i\tfrac{g}{2\cos\theta_W}\gamma^\mu\left[O'^L_{ij}(1-\gamma_5)+O'^R_{ij}(1+\gamma_5)\right]$$

Fig. 4. Feynman rule for the $\chi_i^0\chi_j^0 Z^0$ vertex where the O'_{ij} are a combination of neutralino mass matrices

quarks. This is used as an input, along with the spinors for the light fermions, at the second vertex to calculate the final matrix element for that helicity combination. To obtain the spin-summed matrix element the procedure is repeated for all possible helicities of the external particles. This dramatically reduces the amount of code required for numerical evaluation of the vertices. It also has the additional benefit of providing basis states[3] for the particles that can be stored and passed between the production and decay to ensure that the spin correlations are consistently implemented. Our implementation and the formulation are described in more detail in Appendix A.

3.2 Decayers

The decay of the top described in Sect. 2 is handled by a class that is solely responsible for this decay. When just considering the standard model this is reasonable, since the top is the only heavy fermion[4] present. However, in the case of new physics models there will be a wealth of heavy particles that decay, and creating a class for each decay would be inefficient. Instead we have implemented a set of classes for each set of possible external spin states and each of these classes, called decayers, is responsible for a specific external spin configuration in a decay. At the present time only two-body decays have been considered.[5] Appendix C contains a list of the currently implemented decayer classes.

The standard way in which Herwig++ handles particle decay modes is with a text file listing each mode, along with branching ratios and the object that will handle the decay. We have instead taken the approach of constructing the decay modes and decayer objects automatically. All that is left to the user is to specify the particle(s) that will be decayed. The steps for creating the decay modes and decayer objects are

1. specify the particles for which decay modes are required;
2. analyse each vertex to find whether the particle can interact; if it cannot, skip to the next vertex in the list until one is found that is able to;
3. find the decay products and test whether the decay would be kinematically possible; if not, skip to the next possible mode;
4. if an object already exists that can handle the decay, then assign it to handle the mode, else create a new decayer and assign this to handle the decay.

The created decayer object contains the appropriate code for calculating the matrix element for all possible helicity combinations that can be used in the spin correlation algorithm from Sect. 2.

[3] In this case the spinors for the quarks and light fermions.

[4] Heavy in this context means that it decays before it hadronises.

[5] Any three-body decays read from a decay table are handled with a phase-space decayer and therefore will not include spin correlation information.

There is an additional point to consider when dealing with SUSY models. These models contain additional parameters, such as mixing matrices, that are necessary for vertex calculations. A mechanism has been implemented to read this information from a SUSY Les Houches Accord file [11]. In principle, the file can contain decay modes along with branching ratios. If this is the case, then the decay mode is not created automatically; it is just assigned an appropriate decayer.

In order to be able to decay the particles we must first produce them along with their associated momenta. The next section will describe how this procedure is accomplished within the new framework.

3.3 Hard processes

In the hard process the initial momenta of the outgoing particles from a hard collision are calculated via a leading-order matrix element as in (1). There will be additional PDFs involved if the incoming particles are composite. In Herwig++ the mechanism for this is again "factorised" into pieces concerned with the phase-space evaluation and pieces concerned with the calculation of $|\mathcal{M}|^2$. Here we only concern ourselves with the $2 \to 2$ cross sections and as a result the existing structure only requires us to implement calculations of $|\mathcal{M}|^2$ for the new processes.

Figure 5 shows the possible topologies for a $2 \to 2$ process at tree level. Obviously some processes will not involve all topologies. As in the case for the decayers our approach is not to create a class for each possible process, but instead create classes based on the external spins of the particles involved. The user simply specifies the incoming states and an outgoing particle; all of the possible diagrams with this outgoing particle are then created along with the appropriate MatrixElement object. The object is responsible for calculating the spin-averaged matrix element. In the HELAS approach the matrix element is first calculated by computing the complex amplitude for each diagram of

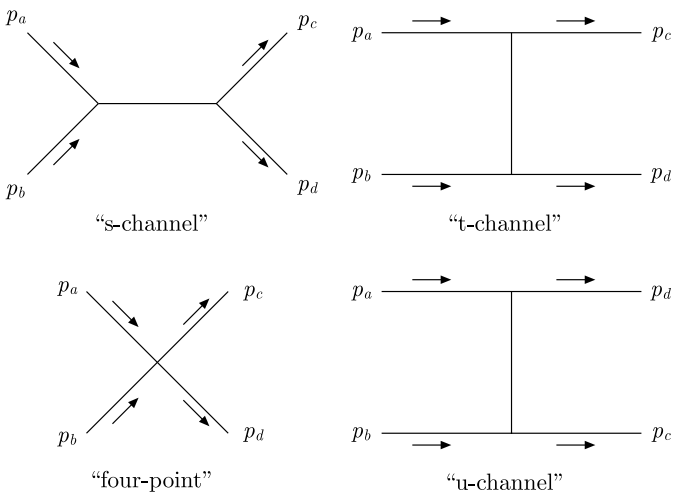

Fig. 5. Tree-level topologies for a $2 \to 2$ process. The *arrows* denote the flow of momenta

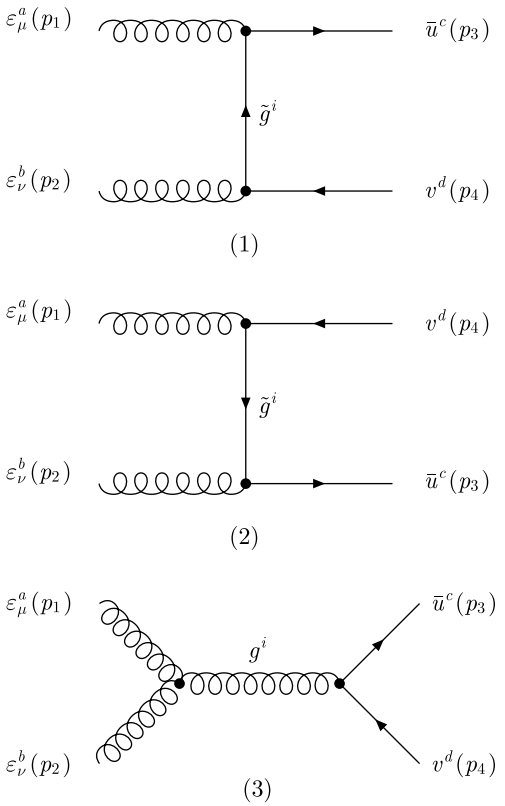

Fig. 6. Diagrams contributing to the process $gg \to \tilde{g}\tilde{g}$ where *lowered Greek letters* denote space-time indices and *raised Roman letters* denote colour indices in the adjoint representation. u and v are the spinors for the gluinos and $\varepsilon_{\mu,\nu}$ are the polarisation vectors of the gluons. The momenta (p_1, p_2) are incoming and (p_3, p_4) are outgoing

a given helicity combination. The diagram contributions are then summed and the modulus squared is taken. This is done for each helicity, and the sum of each helicity gives the spin-summed $|\mathcal{M}|^2$. In the case of strong processes it is easier to separate the colour structure from the evaluation of the matrix element. In a given process the diagrams can be split into "colour flows", which are a combination of diagrams with the same colour structure, reducing the amount of computation required.

To demonstrate this procedure, consider the process $gg \to \tilde{g}\tilde{g}$. The diagrams that contribute are shown in Fig. 6. If the amplitude, stripped of the colour information, for the ith diagram is denoted by $\mathcal{M}_i$, the full amplitude for the 3 diagrams is given by

$$g_1 = \mathrm{i}f^{aci}\mathrm{i}f^{bid}\mathcal{M}_1, \tag{8a}$$
$$g_2 = \mathrm{i}f^{adi}\mathrm{i}f^{bic}\mathcal{M}_2, \tag{8b}$$
$$g_3 = -\mathrm{i}f^{aib}\mathrm{i}f^{icd}\mathcal{M}_3\,, \tag{8c}$$

where g_i denotes the full amplitude and f^{abc} denotes the antisymmetric structure constants.

The factors of i associated with the structure constants are present because of the way the vertex rules are defined within the code. The vertices in Herwig++ are stripped of their colour information and therefore require the extra factors of i to be included, where appropriate, with the colour matrices to give the correct sign.

The combination of structure constants in (8c) can be rewritten using the Jacobi identity to give

$$g_3 = \left(f^{aci}f^{bid} - f^{bci}f^{aid}\right)\mathcal{M}_3\,, \tag{9}$$

making it apparent that the colour structure of the s-channel gluon exchange diagram is simply a combination of the other two colour structures. The full colour amplitude can therefore be written as

$$\mathcal{M}_T = -\left[c_1(\mathcal{M}_1 - \mathcal{M}_3) + c_2(\mathcal{M}_2 + \mathcal{M}_3)\right]\,, \tag{10}$$

where c_i denotes the combination of structure constants from above, and the combination of diagram amplitudes will be known as "colour flows", denoted by f_i. Note that the overall minus sign can be dropped, since it simply corresponds to a phase that will not contribute to the final answer. In order to calculate $|\mathcal{M}|^2$, the constants c_i need to be squared. For the process being considered $|c_1|^2 = |c_2|^2 = N_c^2(N_c^2-1)$ and $c_1c_2^* = c_2c_1^* = N_c^2(N_c^2-1)/2$ where N_c is the number of colours. The spin-summed matrix element, averaged over initial colours and polarisations, is then

$$|\bar{\mathcal{M}}|^2 = \frac{1}{2}\frac{1}{4}\frac{1}{(N_c^2-1)^2}\sum_\lambda C_{ij}f_i^\lambda f_j^{*\lambda}\,, \tag{11}$$

where C_{ij} is a matrix containing the squared colour factors and f_i^λ is the ith colour flow for the set of helicities λ.

As well as calculating $|\mathcal{M}|^2$ for a given process each MatrixElement object is also responsible for setting up the colour structure of the hard process that is required to generate the subsequent QCD radiation and hadronisation. Depending on the colours of the internal and external states involved, there may be more than one possible colour structure for each diagram. For the example in Fig. 6 each diagram has 4 possible colour topologies since the both the gluon and gluino carry a colour and an anticolour line in the large N_c limit. When an event is generated, if this case presents itself, a colour structure is picked at random from the N_t possibilities. While this does rely on using the large N_c limit, we believe it to be a good approximation for the colour structures that we are dealing with.

The possible Majorana nature of external states also gives rise to complications when calculating the matrix element. If the incoming states are a spinor and a barred spinor, then in the case where a u-channel diagram is required two additional spinors must be calculated. The reason for this is that, using the notation of Fig. 5, when c and d are crossed their fermion flow can no longer be reversed, since the initial fermions set the direction in which these arrows point. The two additional spinors required are a spinor for the original outgoing barred state and a barred spinor for the original outgoing spinor state with care being taken to associate the new spinors with the correct helicity.

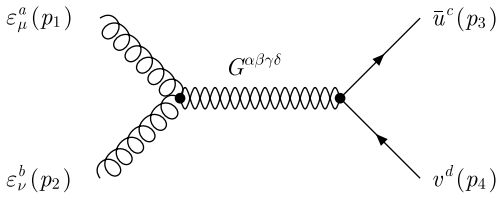

Fig. 7. Resonant graviton exchange from gluon fusion to produce 2 fermions

Appendix B contains a list of the currently implemented MatrixElement classes.[6] The example given above demonstrates a possible SUSY gaugino production process that is taken into account with our new mechanism. We have also implemented another mechanism for the simulation of resonances. This will be described now using an example from the Randall–Sundrum model.

3.4 Resonant processes

Often we are interested in the study of s-channel resonances that decay to standard model particles rather than the production of a new particle in a $2 \to 2$ process. We therefore include a mechanism to study this type of process. We will take as an example here the virtual exchange of a graviton, the lowest lying state of a Kaluza–Klein tower. The graviton is predicted by various models with extra dimensions where gravity is allowed to propagate in the bulk; an example process is shown in Fig. 7. The same matrix element classes as are used to calculate the hard processes are used to calculate the resonant processes. Now, however, there is less computation, since each MatrixElement will contain only a single s-channel diagram and hence a single colour flow.

The next section will detail some physical distributions for the two models discussed previously.

4 Results

The following sections will show some distributions produced using the new BSM code in Herwig++. As there are currently only two models implemented, these will form the basis of the distributions considered.

4.1 Graviton resonances

The LHC may give us the possibility of detecting narrow graviton resonances at the TeV scale through various hard subprocesses. To test our implementation of the RS model we have picked three processes involving graviton exchange: $gg \to G \to e^+e^-$, $u\bar{u} \to G \to e^+e^-$ and $u\bar{u} \to G \to \gamma\gamma$. The plots of the angular distribution of the outgoing fermion/boson with respect to the beam axis in the centre-of-mass frame are shown in Fig. 8. There is good agreement here with the analytical result from the matrix element and the numerical simulation indicating the correct implementation of the graviton Feynman rules and new matrix elements.

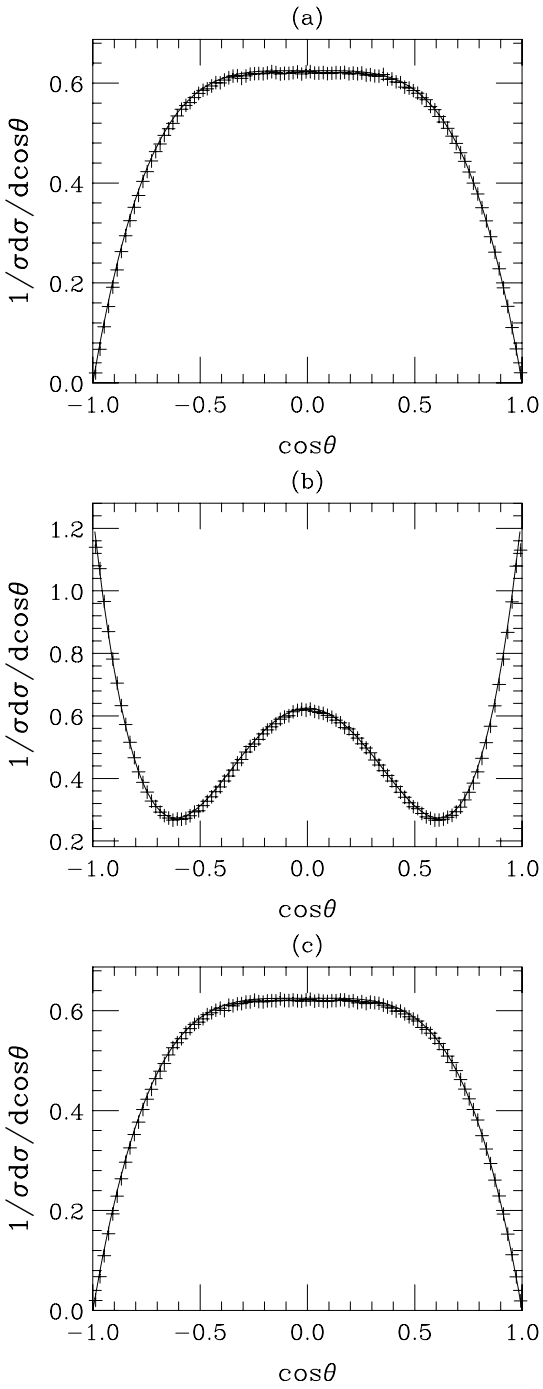

Fig. 8. Angular distributions for fermion and boson production through a resonant graviton. The graviton has a mass of 1 TeV. The *black line* denotes the analytical result and the *crosses* show the simulation data for **a** $gg \to G \to e^+e^-$ **b** $u\bar{u} \to G \to e^+e^-$ and **c** $u\bar{u} \to G \to \gamma\gamma$

These distributions show the characteristic behaviour of an exchanged spin-2 particle. The angular dependence

[6] This includes all of the spin combinations needed in the MSSM and RS model. Additional cases will be implemented when required for a new type of model.

of an exchanged spin-1 boson on the other hand is notably different, and therefore this kind of distribution is extremely useful in identifying the two cases and eliminating possible background spin-1 exchange when searching for this new mode [17] in future experiments. This kind of behaviour may be important for the LHC since Randall–Sundrum type models predict the possibility of narrow graviton resonances at the TeV-scale [18]. Discovery of the kind of behaviour shown in Fig. 8 would certainly be a very strong indication of the existence of some type of extra dimensions model.

4.2 Decay of a squark

The spin correlation algorithm discussed in Sect. 2 was shown to work in the case of $t\bar{t}$ production and decay. One of the simplest cases to consider for a SUSY model is the different decay modes of a left-handed squark. Considering the decay of the squark via the two modes (a) $\tilde{q}_{\mathrm{L}} \to \tilde{\chi}_2^0 q \to \tilde{l}_{\mathrm{R}}^- l^+ u$ and (b) $\tilde{q}_{\mathrm{L}} \to \tilde{\chi}_2^0 q \to \tilde{l}_{\mathrm{R}}^+ l^- u$, and plotting the mass distribution of the produced quark and (anti-) lepton allows the effect of spin correlations to be shown.

The plots in Fig. 9 were produced at Snowmass point 5 [19], where $\tan\beta = 5$, $\mathrm{sign}(\mu) = +$, $M_0 = 150\,\mathrm{GeV}$, $M_2 = 300\,\mathrm{GeV}$ and $A_0 = -1000\,\mathrm{GeV}$. This parameter set gives the following particle spectrum using SOFTSUSY 2.0.8 [20] $M_{\tilde{u}_{\mathrm{L}}} = 672.82\,\mathrm{GeV}$, $M_{\tilde{\chi}_2^0} = 231.29\,\mathrm{GeV}$ and $M_{\tilde{l}_{\mathrm{R}}} = 192.87\,\mathrm{GeV}$.

There is a stark difference in the quark–lepton mass distribution for the two decay modes considered above. The difference is due to the helicities of the external particles. At the mass scale of the squark the quark can be considered massless and left-handed, while the produced lepton and antilepton will be right-handed. When back-to-back the lepton–quark system will have net spin 1 and as such cannot be produced in a scalar decay, while the antilepton–quark system will have spin 0 and is able to proceed.

The end-point in both of the distributions is due to a kinematical cut-off where the invariant mass of the quark–lepton pair is at a maximum. The value of this end-point can be calculated by considering the mass squared when the pair is back-to-back. The value is given in [21] as

$$(m)^2_{\mathrm{max}} = \frac{\left(m^2_{\tilde{u}_l} - m^2_{\tilde{\chi}_2^0}\right)\left(m^2_{\tilde{\chi}_2^0} - m^2_{\tilde{e}_{\mathrm{R}}}\right)}{m^2_{\tilde{\chi}_2^0}}\,. \qquad (12)$$

Using the values for the sparticles above one finds a value for the cut-off of 348.72 GeV, which is consistent with the plots in Fig. 9.

4.3 Gaugino production

Supersymmetry predicts the existence of Majorana fermions and it is necessary to ensure that their spin correlations are implemented correctly in our new framework. We consider three production processes and the angular distributions of the leptons produced in the subsequent decays. The SUSY spectrum for each was again generated using SOFTSUSY, and the masses for the points used in each process are given in the relevant section.

4.3.1 $e^+e^- \to \chi_2^0\chi_1^0$

Here we consider the production of the lightest and next-to-lightest neutralinos with the χ_2^0 decaying via the two modes (i) $\chi_2^0 \to \tilde{l}_{\mathrm{R}}^+ l^- \to l^+ l^- \chi_1^0$, (ii) $\chi_2^0 \to Z^0\chi_1^0 \to l^- l^+ \chi_1^0$ at SPS point 1b. The relevant sparticle masses are $M_{\chi_2^0} =$

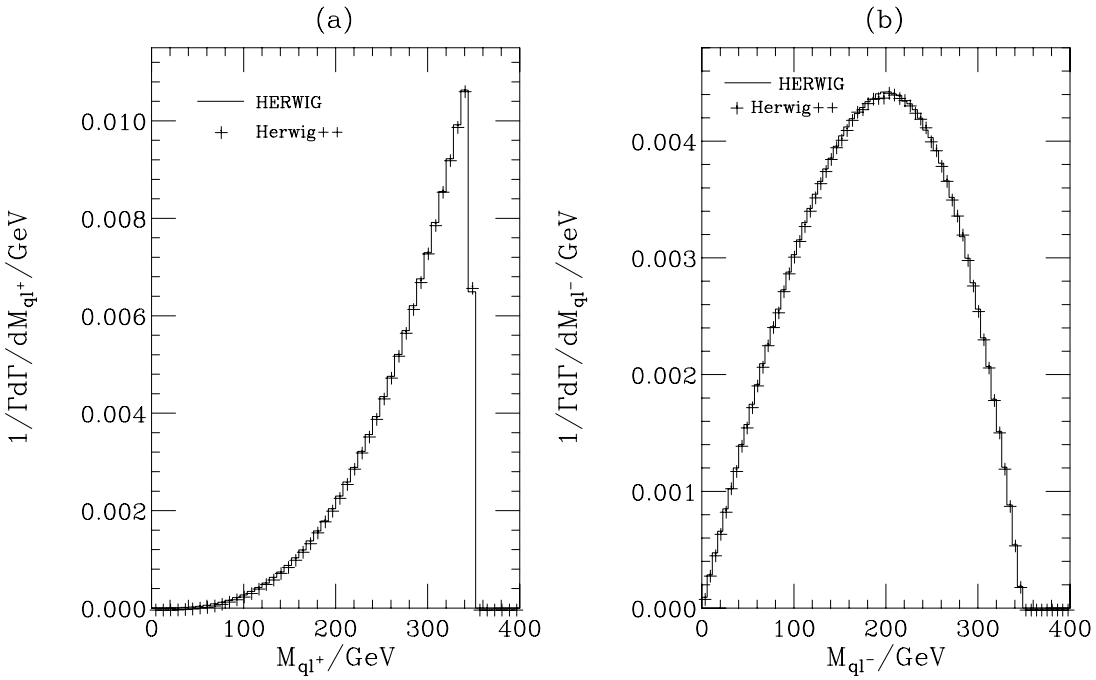

Fig. 9. The invariant mass distribution of **a** the antilepton–quark and **b** lepton–quark produced in $\tilde{u}_{\mathrm{L}} \to \tilde{\chi}_2^0 u \to e^{\pm}\tilde{e}_{\mathrm{R}}^{\mp} u$

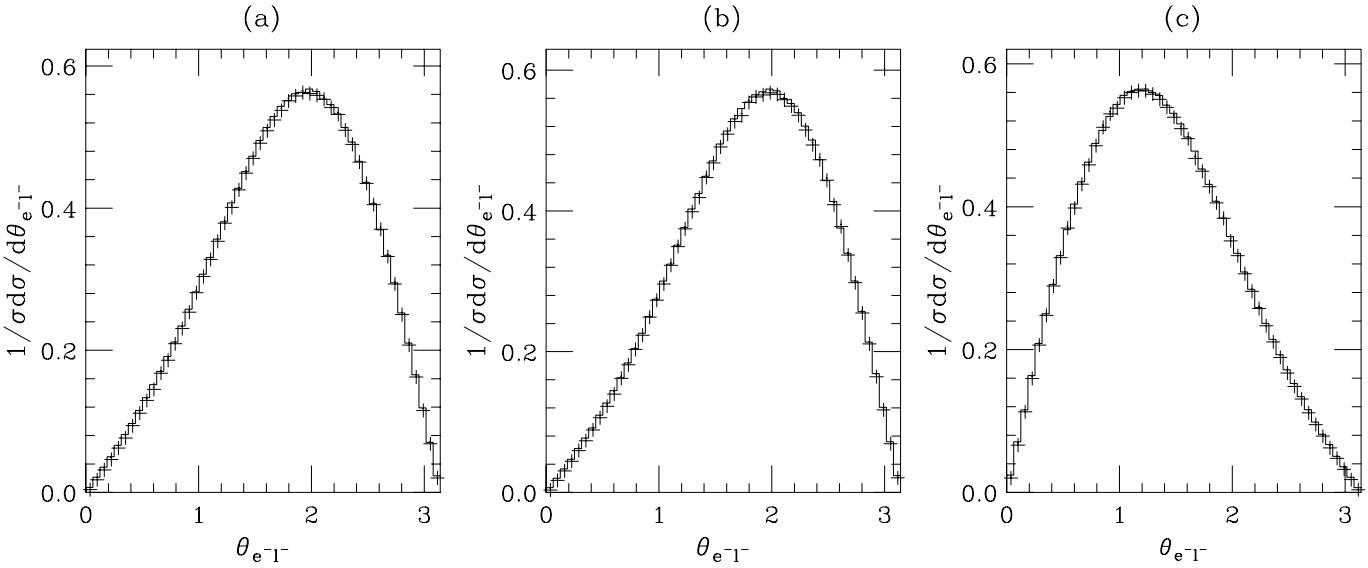

Fig. 10. The angle between the lepton produced in $e^+e^- \to \chi_2^0\chi_1^0 \to \tilde{l}_R^+ l^-$ and the beam in the lab frame for a centre-of-mass energy of 500 GeV and **a** unpolarised incoming beams, **b** negatively polarised electrons and positively polarised positrons and **c** positively polarised electrons and negatively polarised positrons. The *black histogram* is from HERWIG and the *crosses* are from Herwig++

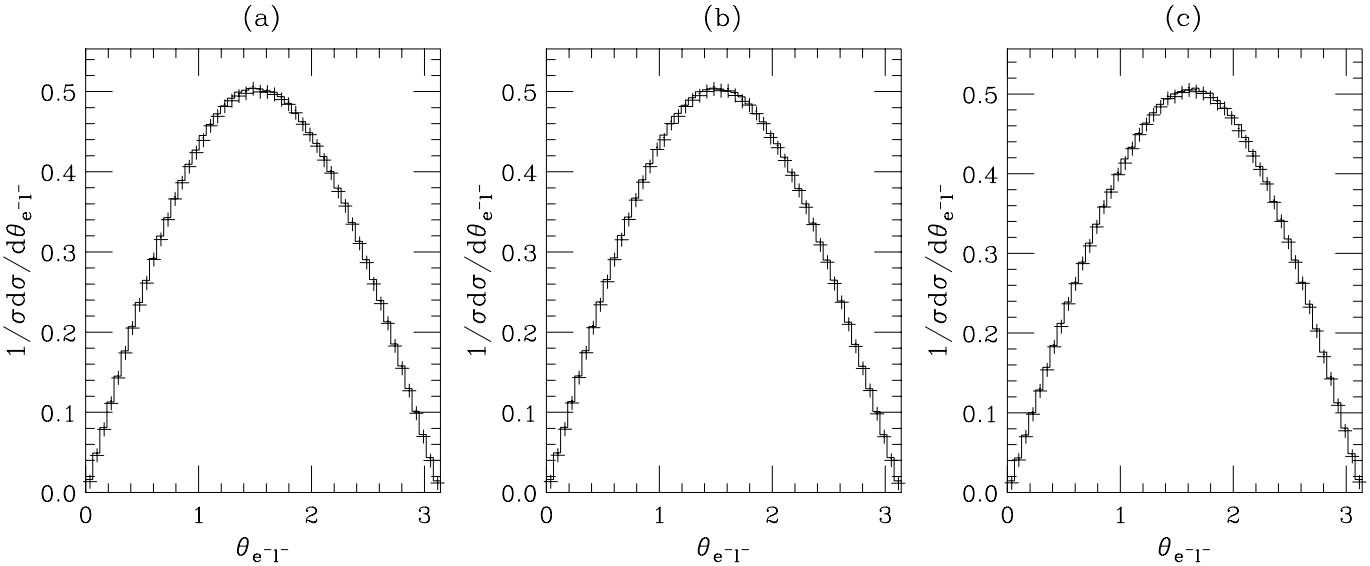

Fig. 11. The angle between the lepton produced in $e^+e^- \to \chi_2^0\chi_1^0 \to Z^0\chi_1^0 \to l^-l^+\chi_1^0$ and the beam in the lab frame for a centre-of-mass energy of 500 GeV and **a** unpolarised incoming beams, **b** negatively polarised electrons and positively polarised positrons and **c** positively polarised electrons and negatively polarised positrons. The *black histogram* is from HERWIG and the *crosses* are from Herwig++

306.55 GeV, $M_{\chi_1^0} = 161.78\,\mathrm{GeV}$, $M_{\tilde{l}_R} = 253.82\,\mathrm{GeV}$. Figure 10 shows how the polarisation of the beam affects the angular distribution of the lepton produced from the χ_2^0 decay.

The lepton shows a correlation with the beam polarisation due to the neutralino being a fermion and preserving spin information when decaying. Figures 11 and 12 show the angular dependence of the final-state lepton for the case of an intermediate Z^0 boson and $\tilde{l}_R$, respectively. As is to be expected for an intermediate slepton, the incoming beam polarisation has little effect on the angular distribution of the final-state lepton due to its scalar nature.[7] The plots are in good agreement with the HERWIG results.

4.3.2 $e^+e^- \to \chi_i^+\chi_i^-$

We now consider the production of chargino pairs and their associated decays. Two possible decay modes of the $\chi_i^\pm$ are

[7] There is some residual effect due to the correlation of the $\tilde{l}_R$ direction with the beam in the χ_2^0 decay.

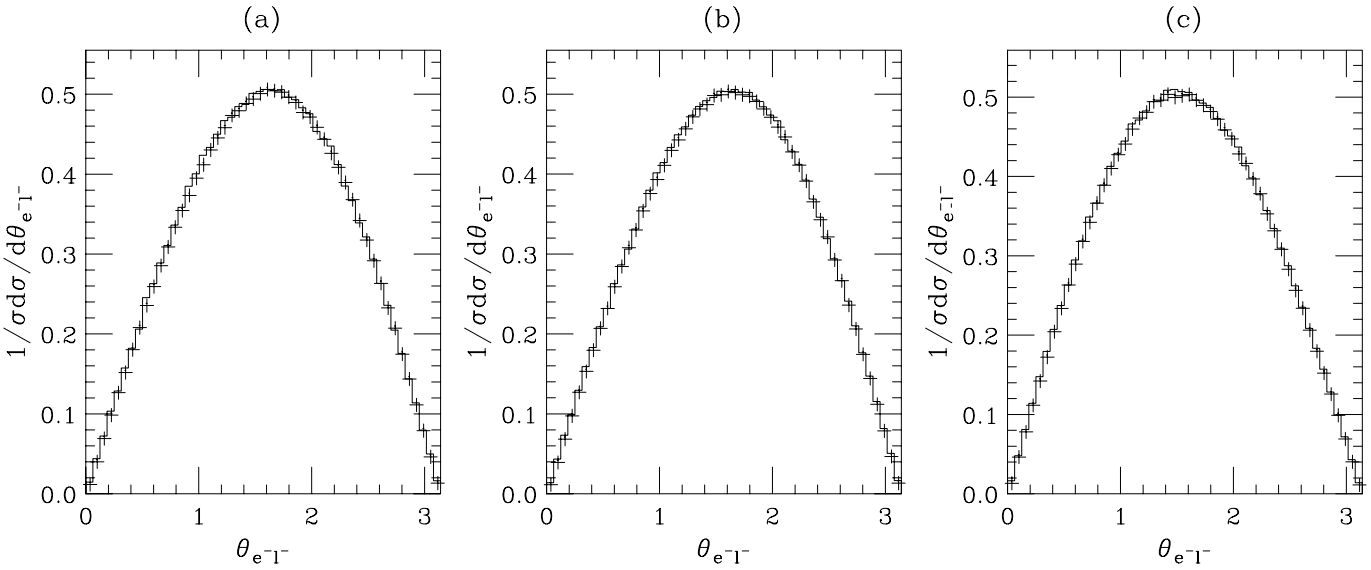

Fig. 12. The angle between the lepton produced in $e^+e^- \to \chi_2^0\chi_1^0 \to \tilde{l}_R^- l^+ \to l^- l^+ \chi_1^0$ and the beam in the lab frame for a centre-of-mass energy of 500 GeV and **a** unpolarised incoming beams, **b** negatively polarised electrons and positively polarised positrons and **c** positively polarised electrons and negatively polarised positrons. The *black histogram* is from HERWIG and the *crosses* are from Herwig++

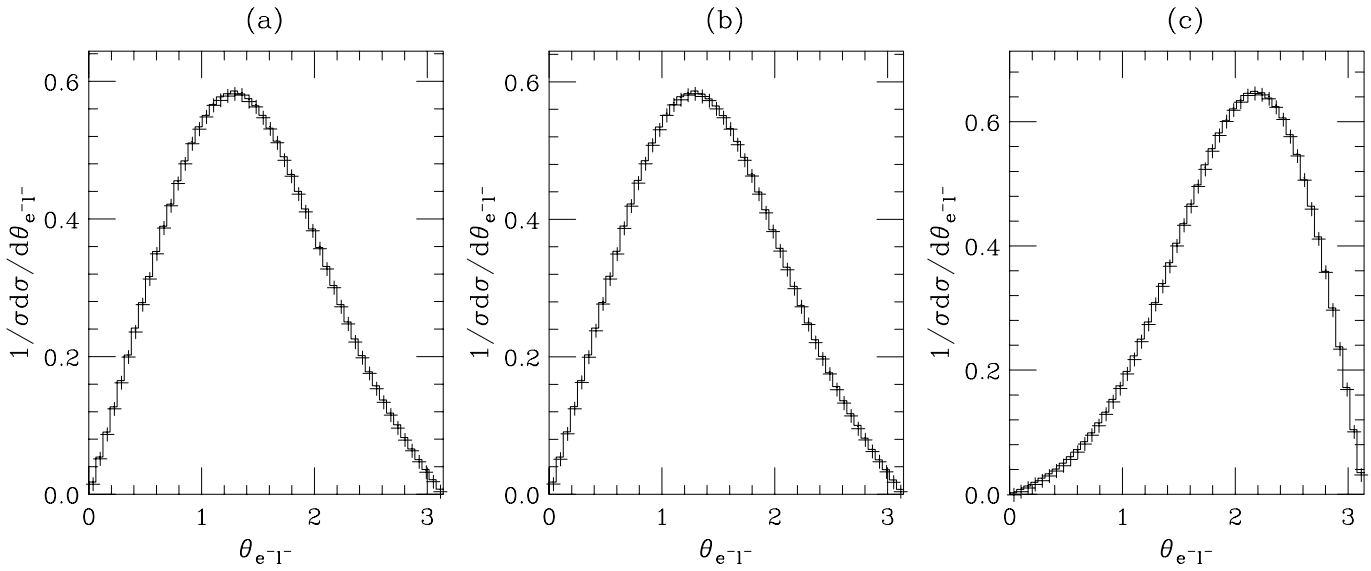

Fig. 13. The angle between the lepton produced in $e^+e^- \to \chi_1^+\chi_1^- \to W^+W^-\chi_1^0\chi_1^0 \to l^- l^+ \nu_l \bar{\nu}_l$ and the beam in the lab frame for a centre-of-mass energy of 500 GeV and **a** unpolarised incoming beams, **b** negatively polarised electrons and positively polarised positrons and **c** positively polarised electrons and negatively polarised positrons. The *black histogram* is from HERWIG and the *crosses* are from Herwig++

(a) $\chi_i^\pm \to W^\pm \chi_1^0$ and (b) $\chi_i^\pm \to \tilde{\nu}_\alpha l^\pm$. Here we use the W decay mode for the lightest chargino and the sneutrino decay mode for the heaviest chargino in order to consider final states with differing spins. The mass spectrum was generated for SPS point 1a, where $M_{\chi_2^+} = 377.39\,\mathrm{GeV}$, $M_{\chi_1^+} = 181.53\,\mathrm{GeV}$, $M_{\tilde{\nu}_L} = 185.42\,\mathrm{GeV}$ and $M_{\chi_1^0} = 97.00\,\mathrm{GeV}$.

Figure 13 shows the angle of the produced electron for the production of the lightest chargino. As is to be expected the beam polarisation affects the lepton distribution, because of the intermediate W boson carrying the spin correlations through to the final state. The effects are similar in the case of the sneutrino decay of the heaviest chargino shown in Fig. 14. The lepton accompanied with the $\tilde{\nu}_L$ still shows correlations with the beam on account of the chargino being a fermion. If the lepton had come from the decay of a scalar, then there would have been no such correlation.

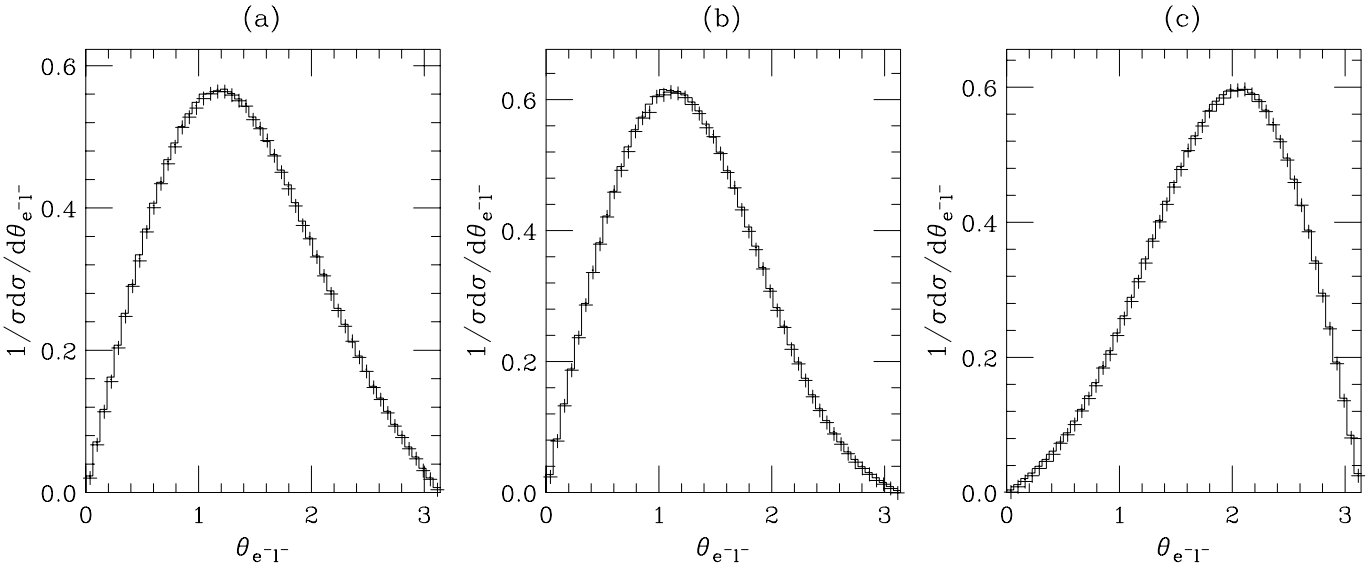

Fig. 14. The angle between the lepton produced in $e^+e^- \to \chi_2^+\chi_2^- \to \tilde{\nu}_L l^+ \tilde{\nu}_L l^-$ and the beam in the lab frame for a centre-of-mass energy of 1 TeV and **a** unpolarised incoming beams, **b** negatively polarised electrons and positively polarised positrons and **c** positively polarised electrons and negatively polarised positrons. The *black histogram* is from HERWIG and the *crosses* are from Herwig++

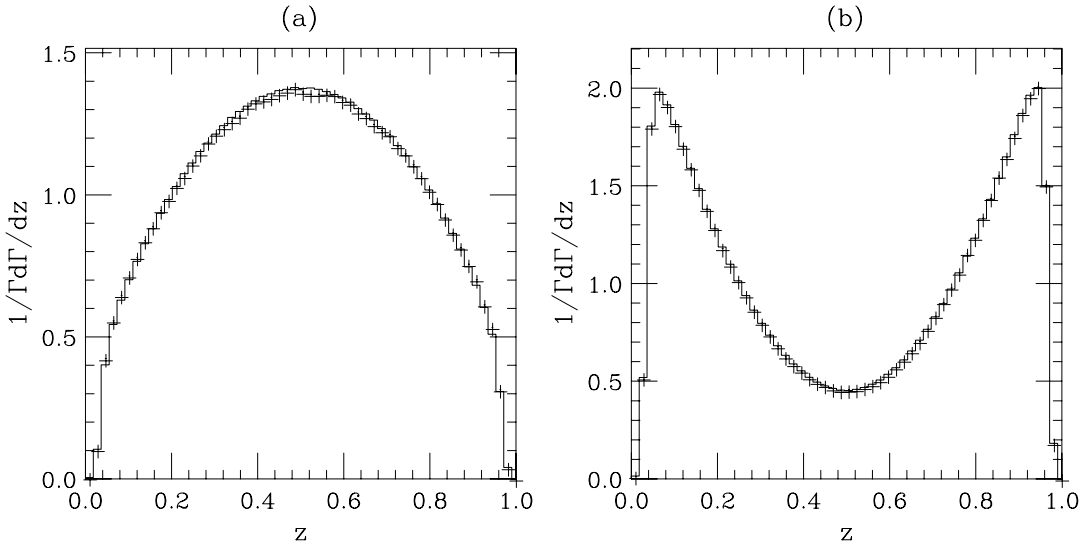

Fig. 15. Energy fraction, z, carried away by the charged meson in the one prong τ decay $\rho^\pm \to \pi^\pm\pi^0$ for **a** left-handed $\tilde{\tau}_1$ and **b** right-handed $\tilde{\tau}_1$. The *black histogram* shows the results from HERWIG with the TAUOLA [24] decay package and the *crosses* indicate the Herwig++results

4.4 Tau decays

4.4.1 One prong decays

The tau has a number of leptonic and hadronic decay modes. A more detailed analysis of these decays shows interesting features in the distribution of energy to the decay products. A typical tau decay involving several mesons has the form $\tau^\pm \to (nm^\pm)(qm^0)\nu_\tau$, where $nm^\pm$ denotes $n \geq 1$ charged mesons, i.e. the number of prongs, and qm^0 denotes $q \geq 0$ neutral mesons. Here we will consider the one prong decay $\tau^\pm \to \rho^\pm\nu_\tau \to \pi^\pm\pi^0\nu_\tau$, where the τ is produced from the decay of a $\tilde{\tau}_1$. Figure 15 shows our results for the fraction of visible energy carried away by the charged meson in the two cases where the $\tilde{\tau}_1$ is (a) 100% left-handed and (b) 100% right-handed.

There is a stark difference in the energy distribution for two possible mixings of the $\tilde{\tau}_1$ in Fig. 15 due to the resulting helicity of the decaying ρ. For the case where the $\tilde{\tau}_1$ is entirely $\tilde{\tau}_L$ the ρ has a higher probability of being transversely polarised, from the results of [25], which favours the equal splitting of energy between the two pions as confirmed by the first plot. A $\tilde{\tau}_1$ that is entirely $\tilde{\tau}_R$, however, will give rise to mostly longitudinally polarised ρ mesons that prefer to distribute their energy unequally and favour a distribution where one meson receives most of the visible energy from the τ decay. This is again confirmed in our second plot. The Herwig++ results are plotted together with those from HERWIG with the TAUOLA decay

package [24], which is designed specifically for the decay of polarised τ leptons.

4.4.2 Decay of a squark

The use of the effects described above in the study of SUSY models has long been recognised. In [23] a mechanism for determining the spin properties of particles involved in SUSY cascade decays using τ polarisation was suggested. The method involves analysing invariant mass distributions of different particle pairs along the decay chain $\tilde{q}_\alpha \to q\chi_2^0 \to \tau^\pm_{\text{near}}\tilde{\tau}_1^\mp \to \tau^\mp_{\text{far}}\chi_1^0$ with the τ decay restricted to $\tau^\pm \to \pi^\pm\nu_\tau$. The various normalised invariant mass distributions are shown in Fig. 16 for $\tilde{q}_\alpha = \tilde{q}_\text{L}$ at SPS point 1a where $M_{\tilde{q}_\text{L}} = 558.4\,\text{GeV}$, $M_{\chi_2^0} = 180.96\,\text{GeV}$, $M_{\tilde{\tau}_1} = 134.56\,\text{GeV}$ and $M_{\chi_1^0} = 97.00\,\text{GeV}$. Since an experiment would be unable to distinguish a near or far τ/π their distributions are combined. The normalisation is to the maximum of the invariant mass. For $m_{\tau\tau}$

$$\left(m^2_{\tau\tau}\right)_{\max} = \left(m^2_{\tilde{\chi}_2^0} - m^2_{\tilde{\tau}_1}\right)\left(1 - m^2_{\tilde{\chi}_1^0}/m^2_{\tilde{\tau}_1}\right) ,$$

which is equal to $(m^2_{\pi\pi})_{\max}$. In the case of the $q\tau$ plots, the maximum of

$$\left(m^2_{\tilde{q}_\text{L}} - m^2_{\tilde{\chi}_2^0}\right)\left(1 - m^2_{\tilde{\tau}_1}/m^2_{\tilde{\chi}_2^0}\right) ,$$
$$\left(m^2_{\tilde{q}_\text{L}} - m^2_{\tilde{\chi}_2^0}\right)\left(1 - m^2_{\tilde{\chi}_2^0}/m^2_{\tilde{\tau}_1}\right) ,$$

is taken, and again this equals $(m^2_{q\pi})_{\max}$.

The differences in shape of the charge conjugate plots in Fig. 16 for the τ and π are due to the different helicities of the τ and π as explained in Sect. 4.2. The kinks in these distributions show the change from near to far leptons or pions making up the main components of the event. Invariant mass distributions of this kind serve as a good indication of the spin properties of the particles involved in cascade decays. This information is important when trying to confirm an exact model of new physics, since it is possible for two different BSM models to imitate each other in certain decays, even though the new particles introduced into each model have different spin assignments [26].

Again our results are plotted along with those from HERWIG using the TAUOLA package. There is excellent

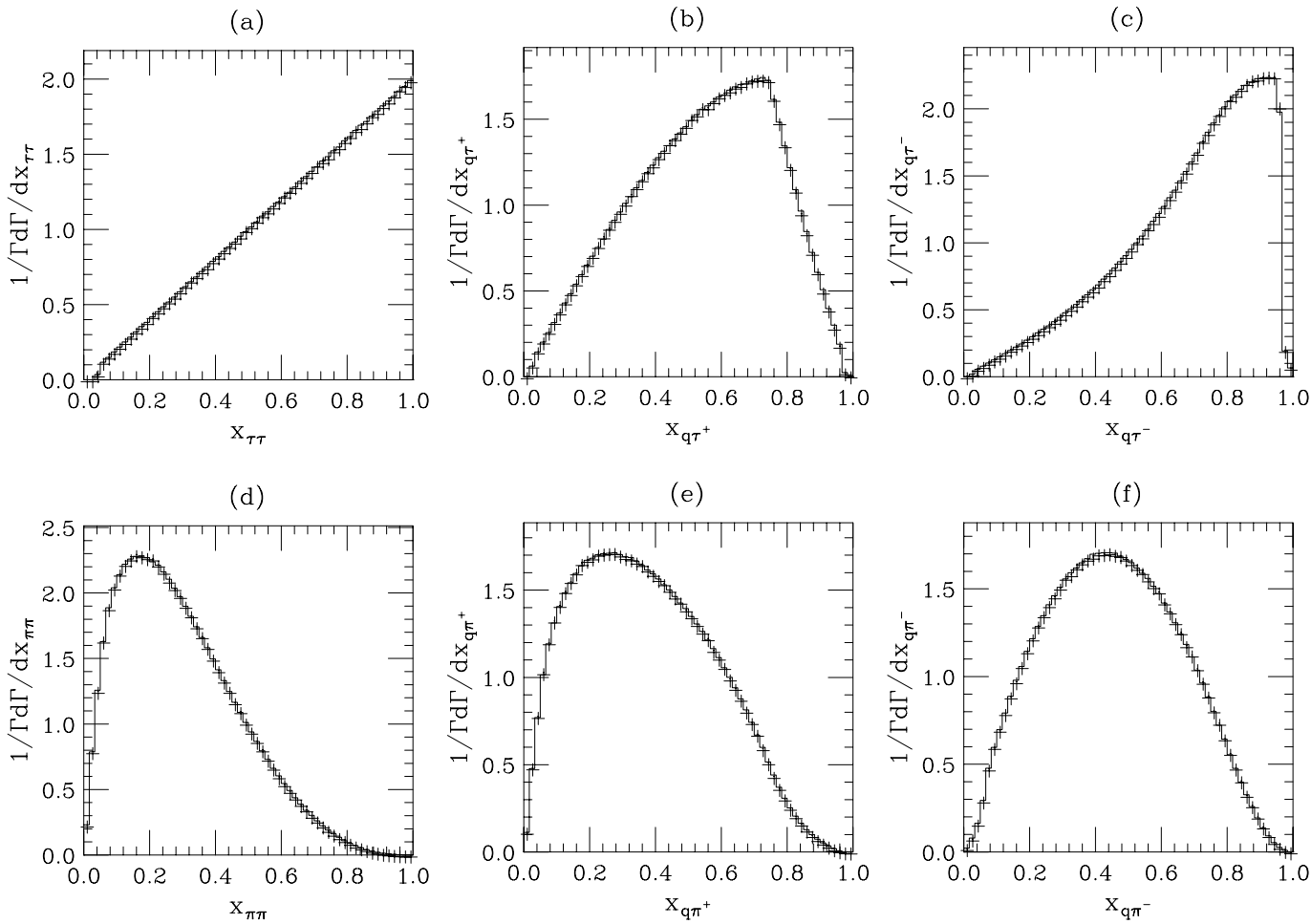

Fig. 16. Normalised invariant mass distributions $x_{ij} = m_{ij}/(m_{ij})_{\max}$ for various pairs of decay products along the chain $\tilde{q}_\alpha \to q\chi_2^0 \to \tau^\pm_{\text{near}}\tilde{\tau}_1^\mp \to \tau^\mp_{\text{far}}\chi_1^0$ where the τ decays via $\tau \to \pi\nu_\tau$ only. The *black histogram* denotes the results from HERWIG with the TAUOLA package and the *crosses* are the results from Herwig++for **a** $\tau\tau$, **b** $q\tau^+$, **c** $q\tau^-$, **d** $\pi\pi$, **e** $q\pi^+$ and **f** $q\pi^-$

agreement between the two sets of results, and the distributions follow those of Fig. 3 in [23].

5 Conclusions

We have described a new method for including new physics models in the Herwig++ event generator that is more general than the previous approach. It allows new models to be implemented with a minimal amount of work. For the models implemented the results are in good agreement with either analytical answers or those from the HERWIG event generator. Any new model will automatically have spin correlations included, since the algorithm demonstrated in Sect. 2 is formulated independently of any specific model and has been shown to agree with expected results.

In the future we plan to implement other BSM physics models in Herwig++, which will enable comparative studies of the phenomenological consequences of these models to be carried out in the framework of the same generator. The current release, 2.0, of Herwig++ [2] does not include any of the features discussed in this paper; it will, however, appear in version 2.1 of the event generator.

Acknowledgements. We would like to thank our collaborators on the Herwig++ project for many useful comments. This work was supported in part by the Science and Technology Facilities Council and the European Union Marie Curie Research Training Network MCnet under contract MRTN-CT-2006-035606.

Appendix A: Helicity code

In the FORTRAN HERWIG program the helicity amplitudes were calculated using the formalism of Kleiss and Stirling [27]. However, this meant that

- all the matrix elements had to be calculated in the same frame;
- it was impossible to interface the correlations in the parton shower and those in the decay of unstable fundamental particles;
- each matrix element had to be separately calculated.

In Herwig++ we choose to use an approach based on the HELAS formalism for the calculation of matrix elements. This approach has a number of advantages:

- we can use the spinors and polarisation vectors calculated when the particle is produced to calculate their decays in a different frame, after an appropriate Lorentz transformation, so that each step of the calculation can be done in the most relevant frame;
- more complicated matrix elements can be calculated from the basic building blocks rather than coded from scratch;
- the inclusion of particles other than scalars, spin-$\frac{1}{2}$ fermions and massless spin-1 bosons, which is complicated in the Kleiss and Stirling formalism, is relatively simple.

The implementation of the HELAS formalism in Herwig++ is based on two fundamental types of objects, WaveFunctionBase and VertexBase.

The WaveFunctions contain the momentum and a pointer to the properties of the particles together with the basis state for a given particle spin. WaveFunctionBase stores the momentum of the particle and a pointer to the ParticleData object for the particle. The inheriting ScalarWaveFunction, SpinorWaveFunction, SpinorBarWaveFunction, VectorWaveFunction, RSSpinorWaveFunction, RSSpinorBarWaveFunction and TensorWaveFunction classes then contain storage of the wave functions for spin-0, -$\frac{1}{2}$, -1, $-\frac{3}{2}$ and -2 particles together with methods to calculate the wave functions for a given helicity state.

The vertex classes contain methods to combine the wave functions for a specific vertex to give either off-shell wave functions, which can be used in further calculations, or the matrix element. The VertexBase class contains storage of the particles that interact at a given vertex. A number of classes then inherit from this class and implement the calculation of the matrix element and off-shell wave functions for a given Lorentz structure of the vertex in terms of arbitrary couplings, which are calculated by virtual member functions.

This strategy is essentially identical to that adopted in the original HELAS approach. However, the new structure has the benefit that the user need only decide which vertex to use with the structure, then supplying the relevant couplings, whereas these had to be specified by hand when using the HELAS library.

A.1 Conventions

To numerically evaluate the matrix elements using the HELAS formalism we need a specific choice of the Dirac matrices; we currently support two options: the conventional low-energy choice, used in for example [28],

$$\gamma_i^{\mathrm{HABER}} = \begin{pmatrix} 0 & \sigma_i \\ -\sigma_i & 0 \end{pmatrix}, \quad \gamma_0^{\mathrm{HABER}} = \begin{pmatrix} 1 & 0 \\ 0 & -1 \end{pmatrix}, \quad \gamma_5^{\mathrm{HABER}} = \begin{pmatrix} 0 & 1 \\ 1 & 0 \end{pmatrix}, \tag{A.1}$$

and the original choice of HELAS, which is more appropriate at high energies,

$$\gamma_i^{\mathrm{HELAS}} = \begin{pmatrix} 0 & \sigma_i \\ -\sigma_i & 0 \end{pmatrix}, \quad \gamma_0^{\mathrm{HELAS}} = \begin{pmatrix} 0 & 1 \\ 1 & 0 \end{pmatrix}, \quad \gamma_5^{\mathrm{HELAS}} = \begin{pmatrix} -1 & 0 \\ 0 & 1 \end{pmatrix}. \tag{A.2}$$

These two representations are related by the transformation

$$\psi_{\mathrm{HELAS}} = S\psi_{\mathrm{Haber}} \quad \text{where} \quad S = \frac{1}{\sqrt{2}} \begin{pmatrix} 1 & -1 \\ 1 & 1 \end{pmatrix}. \tag{A.3}$$

A number of container classes are implemented in the ThePEG framework [29], on which Herwig++ is built, to store the basis states for the different spins:

- LorentzSpinor: storage of the spinor, u or v, for a spin-$\frac{1}{2}$ fermion;
- LorentzSpinorBar: storage of the barred spinor, $\bar{u}$ or $\bar{v}$, for a spin-$\frac{1}{2}$ fermion;
- LorentzPolarizationVector: storage of the polarisation vector, ε^μ, for a spin-1 boson;
- LorentzRSSpinor: storage of the spinor, u^μ or v^μ, for a spin-$\frac{3}{2}$ fermion;
- LorentzRSSpinorBar: storage of the barred spinor, $\bar{u}^\mu$ or $\bar{v}^\mu$, for a spin-$\frac{3}{2}$ fermion;
- LorentzTensor: storage of the polarisation tensor, $\varepsilon^{\mu\nu}$, for a spin-2 boson.

In addition to providing storage of the basis state these classes implement the Lorentz transformations, both boosts and rotations, for the objects. In the case of fermions the Dirac basis used to calculate the spinor, together with whether the spinor is u or v type is also stored. Methods to convert between the two supported Dirac matrix definitions are implemented together with the transformation between u and v spinors for Majorana particles.

A.2 Lorentz transformations

In addition to the storage of the basis states, we need to be able to transform them between different Lorentz frames.

The Lorentz transformation for a spinor is given by

$$\psi'(x') = \psi'(ax) = S(a)\psi(x)\,, \tag{A.4}$$

where $a^\nu_\mu = \frac{\partial x'^\nu}{\partial x^\mu}$. For a Lorentz boost along the direction specified by the unit vector $\hat{\mathbf{n}}$ with a magnitude β the transformation is given by

$$S_{\text{boost}} = \cosh\left(\frac{\chi}{2}\right) + \sinh\left(\frac{\chi}{2}\right)\hat{n}_i\gamma^0\gamma^i\,, \tag{A.5}$$

where $\tanh\chi = \beta$. For a rotation by an angle ϕ about the unit vector $\hat{\mathbf{n}}$ the Lorentz transformation is given by

$$S_{\text{rotation}} = \cos\left(\frac{\phi}{2}\right) + \sin\left(\frac{\phi}{2}\right)\varepsilon^{ijk}\hat{n}_k\gamma^i\gamma^j\,. \tag{A.6}$$

The Lorentz transformations for a four vector is given by

$$\varepsilon^\mu(x') = L(a)^\mu_\nu\varepsilon^\nu(x)\,. \tag{A.7}$$

If we wish to boost by a factor β along a unit vector $\hat{\mathbf{n}}$ the transformation is

$$L^\mu_\nu = \begin{pmatrix} \gamma & -\gamma\beta\hat{n}_1 & -\gamma\beta\hat{n}_2 & -\gamma\beta\hat{n}_3 \\ -\gamma\beta\hat{n}_1 & 1-\hat{n}_1\hat{n}_1\omega & -\hat{n}_1\hat{n}_2\omega & -\hat{n}_1\hat{n}_3\omega \\ -\gamma\beta\hat{n}_2 & -\hat{n}_2\hat{n}_1\omega & 1-\hat{n}_2\hat{n}_2\omega & -\hat{n}_2\hat{n}_3\omega \\ -\gamma\beta\hat{n}_3 & -\hat{n}_3\hat{n}_1\omega & -\hat{n}_3\hat{n}_2\omega & 1-\hat{n}_3\hat{n}_3\omega \end{pmatrix}, \tag{A.8}$$

where $\omega = 1-\gamma$ and $\gamma = \frac{1}{\sqrt{1-\beta^2}}$. The Lorentz transformation for a rotation by an angle δ about a unit vector $\hat{\mathbf{n}}$ is

$$L^\mu_\nu = \begin{pmatrix} 1 & 0 & 0 & 0 \\ 0 & \lambda\hat{n}_1\hat{n}_1 + c_\delta & \lambda\hat{n}_1\hat{n}_2 - s_\delta\hat{n}_3 & \lambda\hat{n}_1\hat{n}_3 + s_\delta\hat{n}_2 \\ 0 & \lambda\hat{n}_2\hat{n}_1 + s_\delta\hat{n}_3 & \lambda\hat{n}_2\hat{n}_2 + c_\delta & \lambda\hat{n}_2\hat{n}_3 - s_\delta\hat{n}_1 \\ 0 & \lambda\hat{n}_3\hat{n}_1 - s_\delta\hat{n}_2 & \lambda\hat{n}_3\hat{n}_2 + s_\delta\hat{n}_1 & \lambda\hat{n}_3\hat{n}_3 + c_\delta \end{pmatrix}, \tag{A.9}$$

where $c_\delta = \cos\delta$, $s_\delta = \sin\delta$ and $\lambda = 1-\cos\delta$. The transformations for the higher-spin particles can then be constructed as products of the spin-$\frac{1}{2}$ and spin-1 transformations, i.e.

$$\psi^\mu(x') = L(a)^\mu_\nu S(a)\psi^\nu(x), \tag{A.10a}$$

$$\varepsilon^{\mu\nu}(x') = L(a)^\mu_\alpha L(a)^\nu_\beta\varepsilon^{\alpha\beta}\,. \tag{A.10b}$$

A.3 WaveFunctions

A.3.1 ScalarWaveFunction

The ScalarWaveFunction class inherits from the WaveFunctionBase class and implements the storage of the wave function of a scalar particle as a complex number. For external particles this is just 1; however, it can assume different values when the WaveFunction is the result is an off-shell internal line from a Vertex class.

A.3.2 SpinorWaveFunction and SpinorBarWaveFunction

As with the ScalarWaveFunction, the SpinorWaveFunction and SpinorBarWaveFunction classes inherit from the WaveFunctionBase class. The spinor is stored as either a LorentzSpinor or LorentzSpinorBar. In addition the calculation of the spinors for external particles is implemented. The spinors are calculated in terms of two-component spinors, as in [16],

$$\chi_+(p) = \frac{1}{\sqrt{2|\mathbf{p}|\,(|\mathbf{p}|+p_z)}}\begin{pmatrix}|\mathbf{p}|+p_z \\ p_x+\mathrm{i}p_y\end{pmatrix}, \tag{A.11a}$$

$$\chi_-(p) = \frac{1}{\sqrt{2|\mathbf{p}|\,(|\mathbf{p}|+p_z)}}\begin{pmatrix}-p_x+\mathrm{i}p_y \\ |\mathbf{p}|+p_z\end{pmatrix}, \tag{A.11b}$$

where $p_{x,y,z}$ are the x, y and z components of the momentum, respectively, E is the energy of the particle and $|\mathbf{p}|$ is the magnitude of the three momentum. For the HELAS choice of the Dirac representation the spinors are given by

$$u(p) = \begin{pmatrix}\omega_{-\lambda}(p)\chi_\lambda(p) \\ \omega_\lambda(p)\chi_\lambda(p)\end{pmatrix}, \tag{A.12a}$$

$$v(p) = \begin{pmatrix}-\lambda\omega_\lambda(p)\chi_{-\lambda}(p) \\ \lambda\omega_{-\lambda}(p)\chi_{-\lambda}(p)\end{pmatrix}, \tag{A.12b}$$

where $\omega_\pm(p) = \sqrt{E\pm|\mathbf{p}|}$ and the helicity $\lambda = \pm 1$. Similarly for the low-energy definition

$$u(p) = \begin{pmatrix}\omega_+(p)\chi_\lambda(p) \\ \lambda\omega_-(p)\chi_\lambda(p)\end{pmatrix}, \tag{A.13a}$$

$$v(p) = \begin{pmatrix}\omega_-(p)\chi_{-\lambda}(p) \\ -\lambda\omega_+(p)\chi_{-\lambda}(p)\end{pmatrix}. \tag{A.13b}$$

A.3.3 VectorWaveFunction

The VectorWaveFunction class inherits from the WaveFunctionBase class and implements the storage of the polarisation vector using the LorentzPolarizationVector class. The polarisation vectors of a spin-1 particle can be calculated using, as in [16],

$$\varepsilon_1^\mu(p) = \frac{1}{|\mathbf{p}|p_T}\left(0, p_x p_z, p_y p_z, -p_T^2\right) , \quad \text{(A.14a)}$$

$$\varepsilon_2^\mu(p) = \frac{1}{p_T}\left(0, -p_y, p_x, 0\right) , \quad \text{(A.14b)}$$

$$\varepsilon_3^\mu(p) = \frac{E}{m|\mathbf{p}|}\left(\frac{|\mathbf{p}|^2}{E}, p_x, p_y, p_z\right) , \quad \text{(A.14c)}$$

where m is the mass and $p_\mathrm{T} = \sqrt{p_x^2 + p_y^2}$. We include two choices of the polarisation vectors:

$$\varepsilon^\mu(p, \lambda = \pm 1) = \frac{1}{\sqrt{2}}\left(\mp\varepsilon_1^\mu(p) - \mathrm{i}\varepsilon_2^\mu(p)\right) , \quad \text{(A.15a)}$$

$$\varepsilon^\mu(p, \lambda = \quad 0) = \varepsilon_3^\mu(p) , \quad \text{(A.15b)}$$

which is the choice used in HELAS. However, while this option is available in the Herwig++ by default we include the additional phase factor $\exp(\mathrm{i}\lambda\phi)$ as in [28] in order to make the inclusion of spin correlations in the parton shower easier.

A.3.4 RSSpinorWaveFunction and RSSpinorBarWaveFunction

Although there are currently no fundamental spin-$\frac{3}{2}$ particles included in Herwig++ the Rarita–Schwinger spinors for spin-$\frac{3}{2}$ particles are included both to allow for the simulation of spin-$\frac{3}{2}$ hadronic resonances and for the possible future inclusion of the gravitino. The RSSpinorWaveFunction and RSSpinorBarWaveFunction inherit from the WaveFunctionBase class and implement the storage of the Rarita–Schwinger spinors using the LorentzRSSpinor and LorentzRSSpinorBar classes, respectively.

The spinors are calculated using the Clebsch–Gordon decomposition:

$$\psi^\mu(p, \lambda = -2) = \varepsilon^\mu(p, -1)\psi(p, -1) ; \quad \text{(A.16a)}$$

$$\psi^\mu(p, \lambda = -1) = \sqrt{\frac{1}{3}}\varepsilon^\mu(p, -1)\psi(p, 1) \quad \text{(A.16b)}$$

$$+ \sqrt{\frac{2}{3}}\varepsilon^\mu(p, 0)\psi(p, -1) ; \quad \text{(A.16c)}$$

$$\psi^\mu(p, \lambda = 1) = \sqrt{\frac{1}{3}}\varepsilon^\mu(p, 1)\psi(p, -1) \quad \text{(A.16d)}$$

$$+ \sqrt{\frac{2}{3}}\varepsilon^\mu(p, 0) ; \quad \text{(A.16e)}$$

$$\psi^\mu(p, \lambda = 2) = \varepsilon^\mu(p, 1)\psi(p, 1) . \quad \text{(A.16f)}$$

For massive particles the spinors are calculated in the rest frame of the particle and then boosted to the required frame in order that the Clebsch–Gordon decomposition can be easily applied. For massless spin-$\frac{3}{2}$ particles, which only have the ± 2 helicity states, the spinors are calculated in the same frame as the momentum.

A.3.5 TensorWaveFunction

The TensorWaveFunction class inherits from the WaveFunctionBase class and implements the storage of the polarisation tensor for spin-2 particles using the LorentzTensor class.

The wave function is calculated using the Clebsch–Gordon decomposition:

$$\varepsilon^{\mu\nu}(p, \lambda = -2) = \varepsilon^\mu(p, -1)\varepsilon^\nu(p, -1) ; \quad \text{(A.17a)}$$

$$\varepsilon^{\mu\nu}(p, \lambda = -1) = \sqrt{\frac{1}{2}}\left[\varepsilon^\mu(p, -1)\varepsilon^\nu(p, 0)\right. \quad \text{(A.17b)}$$

$$\left. + \varepsilon^\mu(p, 0)\varepsilon^\nu(p, -1)\right] ; \quad \text{(A.17c)}$$

$$\varepsilon^{\mu\nu}(p, \lambda = 0) = \sqrt{\frac{1}{2}}[\varepsilon^\mu(p, 1)\varepsilon^\nu(p, -1) + \varepsilon^\mu(p, -1)\varepsilon^\nu(p, 1)$$

$$+ 2\varepsilon^\mu(p, 0)\varepsilon^\nu(p, 0)] ; \quad \text{(A.17d)}$$

$$\varepsilon^{\mu\nu}(p, \lambda = 1) = \sqrt{\frac{1}{2}}\left[\varepsilon^\mu(p, 1)\varepsilon^\nu(p, 0)\right. \quad \text{(A.17e)}$$

$$\left. + \varepsilon^\mu(p, 0)\varepsilon^\nu(p, 1)\right] ; \quad \text{(A.17f)}$$

$$\varepsilon^{\mu\nu}(p, \lambda = 2) = \varepsilon^\mu(p, 1)\varepsilon^\nu(p, 1) . \quad \text{(A.17g)}$$

Here this is applied in the frame in which the momentum is specified.

A.4 Vertices

The Vertices all inherit from the VertexBase class. In general, for all the vertices all the particles and momenta are defined to be incoming.

A.4.1 Scalar vertices

There are a number of vertices involving scalar bosons.

FFSVertex The vertex for the coupling of a fermion and antifermion to a scalar boson is defined to have the perturbative form

$$\mathrm{i}c\bar{f}_2 a^\lambda P_\lambda f_1 \phi_3 , \quad \text{(A.18)}$$

where c is the overall normalisation, a^λ are the left/right couplings, P_λ are the helicity projection operators, f_1 is the wave function for the fermion, $\bar{f}_2$ is the wave function for the antifermion and ϕ_3 is the wave function for the scalar boson.

GeneralSVVVertex In addition, to the perturbative form for the vertex coupling a scalar and two vector bosons described below we include a general form for this interaction, so that effective vertices, for example $h^0 \to gg$, can be implemented. The form of the vertex is

$$\mathrm{i}c\left[a_{00}g^{\mu\nu} + a_{22}p_2^\mu p_2^\nu + a_{23}p_2^\mu p_3^\nu + a_{32}p_3^\mu p_2^\nu + a_{33}p_3^\mu p_3^\nu\right.$$

$$\left. + a_\varepsilon \varepsilon^{\mu\nu\alpha\beta} p_{2\alpha} p_{3\beta}\right] \varepsilon_{2\mu}\varepsilon_{3\nu}\phi_1 , \quad \text{(A.19)}$$

where $p_{2,3}$ are the momenta of the vector bosons, $\varepsilon_{2,3}$ are the wave functions of the vector bosons, ϕ_1 is the wave function of the scalar boson, c is the overall coupling, and a_{ij} are the couplings of the different terms.

SSSVertex The vertex for the coupling of three scalar bosons is defined to have the perturbative form

$$\mathrm{i}c\phi_1\phi_2\phi_3\,, \tag{A.20}$$

where $\phi_{1,2,3}$ are the wave functions for the scalar bosons and c is the coupling.

SSSSVertex The vertex for the coupling of four scalar bosons is defined to have the perturbative form

$$\mathrm{i}c\phi_1\phi_2\phi_3\phi_4\,, \tag{A.21}$$

where $\phi_{1,2,3,4}$ are the wave functions for the scalar bosons and c is the coupling.

VSSVertex The vertex for the coupling of a vector boson and two scalar bosons is defined to have the perturbative form

$$-\mathrm{i}c\,(p_2-p_3)\cdot\varepsilon_1\phi_2\phi_3\,, \tag{A.22}$$

where ε_1 is the wave function of the vector boson, $\phi_{2,3}$ are the wave functions for the scalar bosons and $p_{2,3}$ are the momenta of the scalar bosons, and c is the coupling.

VVSSVertex The vertex for the interaction of two vector and two scalar bosons is defined to have the perturbative form

$$\mathrm{i}cg^{\mu\nu}\varepsilon_{1\mu}\varepsilon_{2\nu}\phi_3\phi_4\,, \tag{A.23}$$

where $\varepsilon_{1,2}$ are the wave functions of the vector bosons and $\phi_{3,4}$ are the wave functions for the scalar bosons and c is the coupling.

VVSVertex The vertex for the interaction of two vector bosons and a scalar boson is defined to have the perturbative form

$$\mathrm{i}cg^{\mu\nu}\varepsilon_{1\mu}\varepsilon_{2\nu}\phi_3\,, \tag{A.24}$$

where $\varepsilon_{1,2}$ are the wave functions of the vector bosons and ϕ_3 is the wave function for the scalar boson, and c is the coupling.

A.4.2 Vector vertices

There are a number of vertices involving vector bosons.

FFVVertex The interaction of a fermion, antifermion and a vector boson is taken to have the perturbative form

$$\mathrm{i}c\bar{f}_2\gamma^\mu a^\lambda P_\lambda f_1\varepsilon_{3\mu}\,, \tag{A.25}$$

where c is the overall normalisation, a^λ are the left/right couplings, f_1 is the wave function for the fermion, $\bar{f}_2$ is the wave function for the antifermion, and ε_3 is the wave function for the vector boson.

VVVVertex The interaction of three vector bosons is taken to have the perturbative form

$$\begin{aligned}&\mathrm{i}g\left[(p_1-p_2)^\gamma g^{\alpha\beta}+(p_2-p_3)^\alpha g^{\beta\gamma}\right.\\&\left.\quad+(p_3-p_1)^\beta g^{\alpha\gamma}\right]\varepsilon_{1\alpha}\varepsilon_{2\beta}\varepsilon_{3\gamma}\,,\end{aligned} \tag{A.26}$$

where $\varepsilon_{1,2,3}$ are the wave functions of the vector bosons and $p_{1,2,3}$ are the momenta of the vector bosons.

VVVVVertex The interaction of four vector bosons is taken to have the form

$$\mathrm{i}c^2\left[2\varepsilon_1\cdot\varepsilon_2\varepsilon_3\cdot\varepsilon_4-\varepsilon_1\cdot\varepsilon_3\varepsilon_2\cdot\varepsilon_4-\varepsilon_1\cdot\varepsilon_4\varepsilon_2\cdot\varepsilon_3\right]\,, \tag{A.27}$$

where $\varepsilon_{1,2,3,4}$ are the wave functions of the vector bosons, and $p_{1,2,3,4}$ are the momenta of the vector bosons. For the quartic gluon vertex this is the contribution of one colour structure. The others can be obtained by an appropriate reordering of the input wave functions.

A.4.3 Tensor vertices

There are a number of vertices involving spin-2 particles. The form of the Feynman rules follows that of [22].

FFTVertex The interaction of a pair of fermions with a tensor is taken to have the perturbative form

$$\begin{aligned}&-\frac{\mathrm{i}\kappa}{8}\bar{f}_2\left[\gamma_\mu(p_1-p_2)_\nu+\gamma_\nu(p_1-p_2)_\mu\right.\\&\left.-2g_{\mu\nu}(\not{p}_1-\not{p}_2)+4g_{\mu\nu}m_f\right]f_1\varepsilon_3^{\mu\nu}\,,\end{aligned} \tag{A.28}$$

where κ is the defined as $2/\Lambda_{\text{cut-off}}$, $p_{1,2}$ are the momenta of the fermions, f_1 is the fermion wave function, $\bar{f}_2$ is the antifermion wave function and $\varepsilon_3^{\mu\nu}$ is the polarisation tensor for the spin-2 particle.

VVVTVertex The interaction of three vector bosons with a tensor is taken to have the perturbative form

$$\begin{aligned}&g\frac{\kappa}{2}\left[C_{\mu\nu,\rho\sigma}(p_1-p_2)_\lambda+C_{\mu\nu,\rho\lambda}(p_3-p_1)_\sigma\right.\\&\left.\quad+C_{\mu\nu,\sigma\lambda}(p_2-p_3)_\rho+F_{\mu\nu,\rho\sigma\lambda}\right]\varepsilon_1^\rho\varepsilon_2^\sigma\varepsilon_3^\lambda\varepsilon_4^{\mu\nu}\,,\end{aligned} \tag{A.29}$$

where κ is $2/\Lambda_{\text{cut-off}}$, $p_{1,2,3}$ are the momenta of the vector bosons, $\varepsilon^\mu_{1,2,3}$ are the polarisation vectors, and $\varepsilon_4^{\mu\nu}$ is the polarisation tensor. The C and F symbols are defined as

$$C_{\mu\nu,\rho\sigma}=g_{\mu\rho}g_{\nu\sigma}+g_{\mu\sigma}g_{\nu\rho}-g_{\mu\nu}g_{\rho\sigma}, \tag{A.30}$$

$$\begin{aligned}F_{\mu\nu,\rho\sigma\lambda}&=g_{\mu\rho}g_{\sigma\lambda}(p_2-p_3)_\nu+g_{\mu\sigma}g_{\rho\lambda}(p_3-p_1)_\nu\\&\quad+g_{\mu\lambda}g_{\rho\sigma}(p_1-p_2)_\nu+(\mu\leftrightarrow\nu)\,.\end{aligned} \tag{A.31}$$

VVTVertex The interaction of two vector bosons with a tensor is taken to have the perturbative form

$$-\frac{\mathrm{i}\kappa}{2}\left[(m_v^2+p_1\cdot p_2)C_{\mu\nu,\rho\sigma}+D_{\mu\nu,\rho\sigma}\right]\varepsilon_1^\rho\varepsilon_2^\sigma\varepsilon_3^{\mu\nu}\,, \tag{A.32}$$

where κ is the defined as $2/\Lambda_{\text{cut-off}}$, m_v is the mass of the gauge boson, $p_{1,2}$ are the momenta of the vector bosons, $\varepsilon^{\mu}_{1,2,3}$ are the polarisation vectors, and $\varepsilon^{\mu\nu}_3$ is the polarisation tensor. The C symbol is defined as above, and D is defined as

$$D_{\mu\nu,\rho\sigma} = g_{\mu\nu}k_{1\sigma}k_{2\rho} - [g_{\mu\sigma}k_{1\nu}k_{2\rho} + g_{\mu\rho}k_{1\sigma}k_{2\nu} - g_{\rho\sigma}k_{1\mu}k_{2\nu} + (\mu \leftrightarrow \nu)] \,. \tag{A.33}$$

FFVTVertex The interaction of a pair of fermions with a vector boson and a tensor is taken to have the perturbative form

$$\frac{\mathrm{i}g\kappa}{4}\bar{f}_2(C_{\mu\nu,\rho\sigma} - g_{\mu\nu}g_{\rho\sigma})\gamma^{\sigma}f_1\varepsilon_3^{\rho}\varepsilon_4^{\mu\nu}\,, \tag{A.34}$$

where κ is the defined as $2/\Lambda_{\text{cut-off}}$, ε_3^{ρ} is the polarisation vector for the boson, f_1 is the fermion wave function, $\bar{f}_2$ is the antifermion wave function, and $\varepsilon_4^{\mu\nu}$ the polarisation tensor for the spin-2 particle. The C symbol is defined above.

SSTVertex The interaction of a pair of scalars with a tensor is taken to have the perturbative form

$$-\frac{\mathrm{i}\kappa}{2}\left[m_S^2 g_{\mu\nu} - p_{1\mu}p_{2\nu} - p_{1\nu}p_{2\mu} + g_{\mu\nu}p_1\cdot p_2\right]\varepsilon_3^{\mu\nu}\phi_1\phi_2\,, \tag{A.35}$$

Table 1. The MatrixElement classes

Class name	Process type
MEff2ff	$\Psi\Psi' \to \Psi''\Psi'''$
MEff2ss	$\Psi\Psi' \to \phi\phi'$
MEff2vv	$\Psi\Psi' \to VV'$
MEfv2fs	$\Psi V \to \Psi\phi$
MEvv2ss	$VV' \to \phi\phi'$
MEvv2ff	$VV' \to \Psi\Psi'$
MEfv2vf	$\Psi V \to V'\Psi'$
MEvv2vv	$VV' \to V''V'''$

Table 2. The two-body decayer classes

Class name	Decay type
FFSDecayer	$\Psi \to \Psi'\phi$
FFVDecayer	$\Psi \to \Psi' V$
SFFDecayer	$\phi \to \Psi\Psi'$
SVVDecayer	$\phi \to VV'$
SSSDecayer	$\phi \to \phi'\phi''$
SSVDecayer	$\phi \to \phi V$
TFFDecayer	$T \to \Psi\Psi'$
TSSDecayer	$T \to \phi\phi'$
TVVDecayer	$T \to VV'$
VFFDecayer	$V \to \Psi\Psi'$
VSSDecayer	$V \to \phi\phi'$
VVVDecayer	$V \to V'V''$

where κ is the defined as $2/\Lambda_{\text{cut-off}}$, $\Lambda_{\text{cut-off}}$ is the ultraviolet cut-off scale, m_S is the mass of the scalar, $p_{1,2}$ are the momenta of the scalars, $\varepsilon_3^{\mu\nu}$ is the polarisation tensor for the spin-2 particle, and $\phi_{1,2}$ are the scalar wave functions.

Appendix B: MatrixElement classes

Table 1 gives a list of the implemented $2 \to 2$ MatrixElement classes with a description of the types of hard subprocess they can handle. Ψ stands for a fermion, V for a vector boson and ϕ for a scalar. Charge conjugate modes are handled by the class responsible for the standard mode.

Appendix C: Decayer classes

Table 2 is a list of the implemented two-body decayer classes with a description of the types of decay that they are designed to handle. Ψ stands for a fermion, V for a vector boson, ϕ for a scalar and T for a tensor. Charge conjugate modes are handled by the class responsible for the standard decay mode.

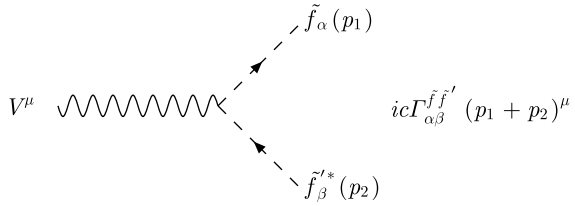

Fig. 17. Feynman rule for the interaction of a gauge boson with a pair of sfermions. The definition of Γ for the various types of gauge boson and sfermion is given in Table 3. The momenta are to be taken as in the direction of the *arrows*

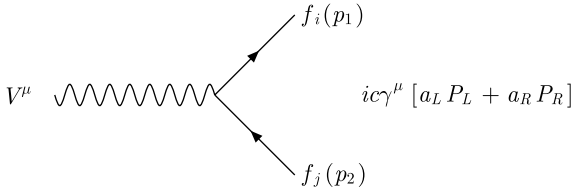

Fig. 18. Feynman rule for the interaction of a gauge boson and a pair of gauginos. The couplings are defined in Table 4

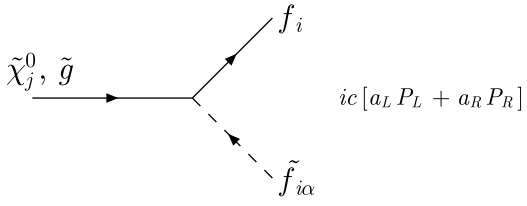

Fig. 19. Feynman rule of the coupling of the neutralinos and gluino with a standard model fermion and an sfermion. Table 5 gives the definitions of a_{L} and a_{R}

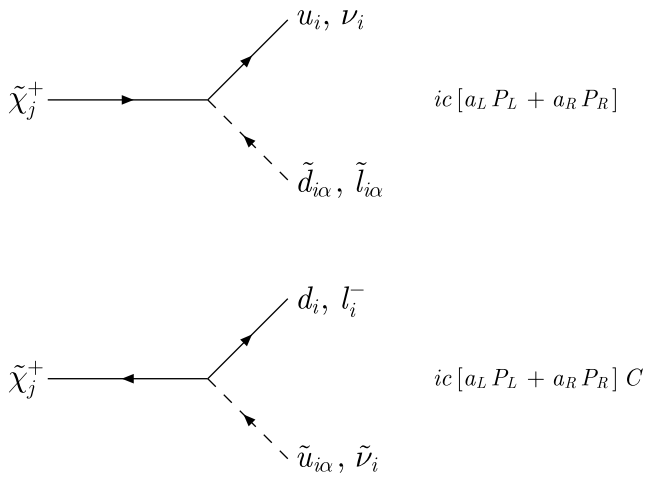

Fig. 20. Feynman rule of the coupling of a chargino with a standard model fermion and an sfermion. C is the charge conjugation matrix. Table 6 gives the definitions of a_{L} and a_{R}

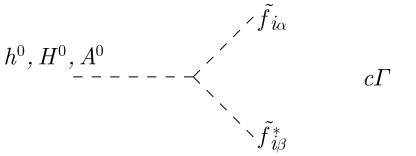

Fig. 21. Feynman rule for the coupling of two gluons to a pair of squarks

Appendix D: Implemented vertices

Below is a list of vertices and associated Feynman rules, for BSM physics, as they are currently implemented. The rules involving colour are written with the colour dependence explicitly pulled to the front , since this is not included in the code for a specific vertex as explained in Sect. 3.3. If a structure constant f^{abc} is involved, an additional factor of i is pulled out along with it due to the commutator relation $\left[t^a, t^b\right] = \mathrm{i} f^{abc} t^c$.

D.1 RSModel

The Feynman rules as implemented in Herwig++ are given in Appendix A.4.3.

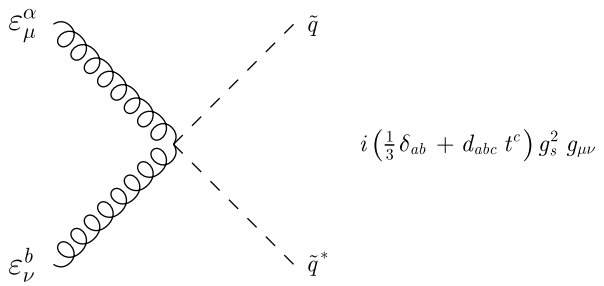

Fig. 22. Feynman rule for the coupling of a Higgs particle with a pair of sfermions. The definition of Γ for the three neutral Higgs bosons are given in Tables 7–9

Table 3. Couplings for the gauge bosons and sfermions

V^μ	$\tilde{f}\tilde{f}'$	c	$\Gamma^{\tilde{f}\tilde{f}'}_{\alpha\beta}$
γ	$\tilde{q}\tilde{q}'$	$-ee_q$	$\delta^{\tilde{q}\tilde{q}'}_{\alpha\beta}$
γ	$\tilde{l}\tilde{l}'$	e	$\delta^{\tilde{l}\tilde{l}'}_{\alpha\beta}$
g	$\tilde{q}\tilde{q}'$	$-gt^a$	$\delta^{\tilde{q}\tilde{q}'}_{\alpha\beta}$
Z^0	$\tilde{u}_\alpha\tilde{u}_\beta$	$\frac{g}{\cos\theta_{\mathrm{W}}}$	$\frac{1}{2}\left(-Q^{2i}_{1\alpha}Q^{2i}_{1\beta} + 2e_u\sin^2\theta_{\mathrm{W}}\delta_{\alpha\beta}\right)$
Z^0	$\tilde{d}_\alpha\tilde{d}_\beta$	$\frac{g}{\cos\theta_{\mathrm{W}}}$	$\frac{1}{2}\left(Q^{2i-1}_{1\alpha}Q^{2i-1}_{1\beta} + 2e_d\sin^2\theta_{\mathrm{W}}\delta_{\alpha\beta}\right)$
Z^0	$\tilde{l}_\alpha\tilde{l}_\beta$	$\frac{g}{\cos\theta_{\mathrm{W}}}$	$\frac{1}{2}\left(L^{2i-1}_{1\alpha}L^{2i-1}_{1\beta} - 2\sin^2\theta_{\mathrm{W}}\delta_{\alpha\beta}\right)$
Z^0	$\tilde{\nu}_\alpha\tilde{\nu}_\beta$	$\frac{g}{\cos\theta_{\mathrm{W}}}$	$-\frac{1}{2}\delta_{11}$
W^-	$\tilde{q}_\alpha\tilde{q}'_\beta$	$\frac{-g}{\sqrt{2}}$	$Q^{2i}_{1\alpha}Q^{2i-1}_{1\beta}$
W^-	$\tilde{\nu}\tilde{l}_\beta$	$\frac{-g}{\sqrt{2}}$	$L^{2i-1}_{1\beta}$

D.2 MSSM

We give the Feynman rules for the MSSM as implemented in Herwig++. These are shown in Figs. 17–22. The sfermion mixing matrices are denoted by $Q^k_{\alpha\beta}$ and $L^k_{\alpha\beta}$ for the squarks and leptons, respectively, where k is the generation number, α the left/right eigenstate and β the mass eigenstate. N_{ij}, U_{ij} and V_{ij} are the neutralino and chargino mixing matrices, respectively. The primed matrices in the

Table 4. Feynman rules for the coupling of a gauge boson to a pair of electroweak gauginos. All momenta are to be taken as outgoing

V^μ	$\tilde{f}\tilde{f}'$	c	a_{L}	a_{R}
γ	$\tilde{\chi}_i^+\tilde{\chi}_j^-$	$-e$	1	1
W^+	$\tilde{\chi}_i^0\tilde{\chi}_j^+$	g	$-\frac{1}{\sqrt{2}}N_{i4}V^*_{j2} + N_{i2}V^*_{j1}$	$\frac{1}{\sqrt{2}}N^*_{i3}U_{j2} + N^*_{i2}U_{j1}$
Z^0	$\tilde{\chi}_i^0\tilde{\chi}_j^0$	$\frac{g}{\cos\theta_{\mathrm{W}}}$	$-\frac{1}{2}N_{i3}N^*_{j3} + \frac{1}{2}N_{i4}N^*_{j4}$	$-a^*_L$
Z^0	$\tilde{\chi}_i^-\tilde{\chi}_j^+$	$\frac{g}{\cos\theta_{\mathrm{W}}}$	$-V_{i1}V^*_{j1} - \frac{1}{2}V_{i2}V^*_{j2}$	$-U^*_{i1}U_{j1} - \frac{1}{2}U^*_{i2}U_{j2}$
			$+\delta_{ij}\sin^2\theta_{\mathrm{W}}$	$+\delta_{ij}\sin^2\theta_{\mathrm{W}}$
g_a	$\tilde{g}_b\tilde{g}_c$	$\{\mathrm{i}f_{abc}\}\,g_s$	1	1

Table 5. Neutralino and gluino couplings. In the case of the gluino $k = 2i$ for up-type quarks and $k = 2i-1$ for down-type quarks

$f_i\tilde{f}_{i\alpha}$	c	
$u_i\tilde{u}_{i\alpha}$	$-\sqrt{2}$	$a_{\mathrm{L}} : \frac{gm_{u_i}N^*_{j4}}{2M_W \sin\beta}Q^{2i}_{1\alpha} - Q^{2i}_{2\alpha}\left(ee_u N'^*_{j1} - \frac{ge_u \sin^2\theta_{\mathrm{W}} N'^*_{j2}}{\cos\theta_{\mathrm{W}}}\right)$
		$a_{\mathrm{R}} : \frac{gm_{u_i}N_{j4}}{2M_W \sin\beta}Q^{2i}_{2\alpha} + Q^{2i}_{1\alpha}\left(ee_u N'_{j1} + \frac{g\left(\frac{1}{2} - e_u \sin^2\theta_{\mathrm{W}}\right)N'_{j2}}{\cos\theta_{\mathrm{W}}}\right)$
$d_i\tilde{d}_{i\alpha}$	$-\sqrt{2}$	$a_{\mathrm{L}} : \frac{gm_{d_i}N^*_{j3}}{2M_W \cos\beta}Q^{2i-1}_{1\alpha} - Q^{2i-1}_{2\alpha}\left(ee_d N'^*_{j1} - \frac{ge_d \sin^2\theta_{\mathrm{W}} N'^*_{j2}}{\cos\theta_{\mathrm{W}}}\right)$
		$a_{\mathrm{R}} : \frac{gm_{d_i}N_{j3}}{2M_W \cos\beta}Q^{2i-1}_{2\alpha} + Q^{2i-1}_{1\alpha}\left(ee_d N'_{j1} - \frac{g\left(\frac{1}{2} + e_d \sin^2\theta_{\mathrm{W}}\right)N'_{j2}}{\cos\theta_{\mathrm{W}}}\right)$
$l_i\tilde{l}_{i\alpha}$	$-\sqrt{2}$	$a_{\mathrm{L}} : \frac{gm_{l_i}N^*_{j3}}{2M_W \cos\beta}L^{2i-1}_{1\alpha} + L^{2i-1}_{2\alpha}\left(eN'^*_{j1} - \frac{g \sin^2\theta_{\mathrm{W}}}{\cos\theta_{\mathrm{W}}}N'^*_{j2}\right)$
		$a_{\mathrm{R}} : \frac{gm_{l_i}N_{j3}}{2M_W \cos\beta}L^{2i-1}_{2\alpha} - L^{2i-1}_{1\alpha}\left(eN'_{j1} + \frac{g\left(\frac{1}{2} - \sin^2\theta_{\mathrm{W}}\right)}{\cos\theta_{\mathrm{W}}}N'_{j2}\right)$
$\nu_i\tilde{\nu}_i$	$-\sqrt{2}$	$a_{\mathrm{L}} : 0 \quad a_{\mathrm{R}} : \frac{gN'_{j2}}{2\cos\theta_{\mathrm{W}}}$
$q^b_i\tilde{q}^c_{i\alpha}$	$\{t^a_{bc}\}\,(-g_s\sqrt{2})$	$a_{\mathrm{L}} : -Q^k_{2\alpha} \quad a_{\mathrm{R}} : Q^k_{1\alpha}$

Table 6. Chargino couplings for the ith fermion generation

$f_i\tilde{f}'_{i\alpha}$	c	a_{L}	a_{R}
$u_i\tilde{d}_{i\alpha}$	$-g$	$-\frac{m_{u_i}V^*_{j2}}{\sqrt{2}M_W \sin\beta}Q^{2i-1}_{1\alpha}$	$U_{j1}Q^{2i-1}_{1\alpha} - \frac{m_{d_i}U_{j2}}{\sqrt{2}M_W \cos\beta}Q^{2i-1}_{2\alpha}$
$d_i\tilde{u}_{i\alpha}$	$-g$	$-\frac{m_{d_i}U^*_{j2}}{\sqrt{2}M_W \cos\beta}Q^{2i}_{1\alpha}$	$V_{j1}Q^{2i}_{1\alpha} - \frac{m_{u_i}V_{j2}}{\sqrt{2}M_W \sin\beta}Q^{2i}_{2\alpha}$
$\nu_i\tilde{l}_{i\alpha}$	$-g$	0	$U_{j1}L^{2i-1}_{1\alpha} - \frac{m_{l_i}U_{j2}}{\sqrt{2}M_W \cos\beta}L^{2i-1}_{2\alpha}$
$l_i\tilde{\nu}_{i\alpha}$	$-g$	$-\frac{m_{l_i}U^*_{j2}}{\sqrt{2}M_W \cos\beta}$	V_{j1}

Table 7. h^0 couplings to sfermion pairs with $c = \mathrm{i}g$

$\tilde{f}_{i\alpha}\tilde{f}^*_{i\beta}$	Γ
$\tilde{u}_{i\alpha}\tilde{u}^*_{i\beta}$	$\frac{M_Z \sin(\alpha+\beta)}{\cos\theta_{\mathrm{W}}}\left[Q^{2i}_{1\alpha}Q^{2i}_{1\beta}\left(\frac{1}{2} - e_u \sin^2\theta_{\mathrm{W}}\right) + e_u \sin^2\theta_{\mathrm{W}}Q^{2i}_{2\alpha}Q^{2i}_{2\beta}\right]$
	$-\frac{m^2_{u_i}\cos\alpha}{M_W \sin\beta}\left[Q^{2i}_{1\alpha}Q^{2i}_{1\beta} + Q^{2i}_{2\alpha}Q^{2i}_{2\beta}\right]$
	$-\frac{m_{u_i}}{2M_W \sin\beta}\left(A_{u_i}\cos\alpha + \mu\sin\alpha\right)\left[Q^{2i}_{2\alpha}Q^{2i}_{1\beta} + Q^{2i}_{1\alpha}Q^{2i}_{2\beta}\right]$
$\tilde{d}_{i\alpha}\tilde{d}^*_{i\beta}$	$-\frac{M_Z \sin(\alpha+\beta)}{\cos\theta_{\mathrm{W}}}\left[Q^{2i-1}_{1\alpha}Q^{2i-1}_{1\beta}\left(\frac{1}{2} + e_d \sin^2\theta_{\mathrm{W}}\right) - e_d \sin^2\theta_{\mathrm{W}}Q^{2i-1}_{2\alpha}Q^{2i-1}_{2\beta}\right]$
	$+\frac{m^2_{d_i}\sin\alpha}{M_W \cos\beta}\left[Q^{2i-1}_{1\alpha}Q^{2i-1}_{1\beta} + Q^{2i-1}_{2\alpha}Q^{2i-1}_{2\beta}\right]$
	$+\frac{m_{d_i}}{2M_W \cos\beta}\left(A_{d_i}\sin\alpha + \mu\cos\alpha\right)\left[Q^{2i-1}_{2\alpha}Q^{2i-1}_{1\beta} + Q^{2i-1}_{1\alpha}Q^{2i-1}_{2\beta}\right]$
$\tilde{l}_{i\alpha}\tilde{l}^*_{i\beta}$	$-\frac{M_Z \sin(\alpha+\beta)}{\cos\theta_{\mathrm{W}}}\left[L^{2i-1}_{1\alpha}L^{2i-1}_{1\beta}\left(\frac{1}{2} - \sin^2\theta_{\mathrm{W}}\right) + \sin^2\theta_{\mathrm{W}}L^{2i-1}_{2\alpha}L^{2i-1}_{2\beta}\right]$
	$+\frac{m^2_{l_i}\sin\alpha}{M_W \cos\beta}\left[L^{2i-1}_{1\alpha}L^{2i-1}_{1\beta} + L^{2i-1}_{2\alpha}L^{2i-1}_{2\beta}\right]$
	$+\frac{m_{l_i}}{2M_W \cos\beta}\left(A_{e_i}\sin\alpha + \mu\cos\alpha\right)\left[L^{2i-1}_{2\alpha}L^{2i-1}_{1\beta} + L^{2i-1}_{1\alpha}L^{2i-1}_{2\beta}\right]$
$\tilde{\nu}_{i\alpha}\tilde{\nu}^*_{i\beta}$	$\frac{M_Z \sin(\alpha+\beta)}{2\cos\theta_{\mathrm{W}}}$

Table 8. H^0 couplings to sfermion pairs with $c = \mathrm{i}g$

$\tilde{f}_{i\alpha}\tilde{f}^*_{i\beta}$	Γ
$\tilde{u}_{i\alpha}\tilde{u}^*_{i\beta}$	$-\frac{M_Z\cos(\alpha+\beta)}{\cos\theta_\mathrm{W}}\left[Q^{2i}_{1\alpha}Q^{2i}_{1\beta}\left(\frac{1}{2}-e_u\sin^2\theta_\mathrm{W}\right)+e_u\sin^2\theta_\mathrm{W}Q^{2i}_{2\alpha}Q^{2i}_{2\beta}\right]$
	$-\frac{m^2_{u_i}\sin\alpha}{M_W\sin\beta}\left[Q^{2i}_{1\alpha}Q^{2i}_{1\beta}+Q^{2i}_{2\alpha}Q^{2i}_{2\beta}\right]$
	$-\frac{m_{u_i}}{2M_W\sin\beta}\left(A_{u_i}\sin\alpha-\mu\cos\alpha\right)\left[Q^{2i}_{2\alpha}Q^{2i}_{1\beta}+Q^{2i}_{1\alpha}Q^{2i}_{2\beta}\right]$
$\tilde{d}_{i\alpha}\tilde{d}^*_{i\beta}$	$\frac{M_Z\cos(\alpha+\beta)}{\cos\theta_\mathrm{W}}\left[Q^{2i-1}_{1\alpha}Q^{2i-1}_{1\beta}\left(\frac{1}{2}+e_d\sin^2\theta_\mathrm{W}\right)-e_d\sin^2\theta_\mathrm{W}Q^{2i-1}_{2\alpha}Q^{2i-1}_{2\beta}\right]$
	$-\frac{m^2_{d_i}\cos\alpha}{M_W\cos\beta}\left[Q^{2i-1}_{1\alpha}Q^{2i-1}_{1\beta}+Q^{2i-1}_{2\alpha}Q^{2i-1}_{2\beta}\right]$
	$+\frac{m_{d_i}}{2M_W\cos\beta}\left(\mu\sin\alpha-A_{d_i}\cos\alpha\right)\left[Q^{2i-1}_{2\alpha}Q^{2i-1}_{1\beta}+Q^{2i-1}_{1\alpha}Q^{2i-1}_{2\beta}\right]$
$\tilde{l}_{i\alpha}\tilde{l}^*_{i\beta}$	$\frac{M_Z\cos(\alpha+\beta)}{\cos\theta_\mathrm{W}}\left[L^{2i-1}_{1\alpha}L^{2i-1}_{1\beta}\left(\frac{1}{2}-\sin^2\theta_\mathrm{W}\right)+\sin^2\theta_\mathrm{W}L^{2i-1}_{2\alpha}L^{2i-1}_{2\beta}\right]$
	$-\frac{m^2_{l_i}\cos\alpha}{M_W\cos\beta}\left[L^{2i-1}_{1\alpha}L^{2i-1}_{1\beta}+L^{2i-1}_{2\alpha}L^{2i-1}_{2\beta}\right]$
	$+\frac{m_{l_i}}{2M_W\cos\beta}\left(\mu\sin\alpha-A_{e_i}\cos\alpha\right)\left[L^{2i-1}_{2\alpha}L^{2i-1}_{1\beta}+L^{2i-1}_{1\alpha}L^{2i-1}_{2\beta}\right]$
$\tilde{\nu}_{i\alpha}\tilde{\nu}^*_{i\beta}$	$-\frac{M_Z\cos(\alpha+\beta)}{2\cos\theta_\mathrm{W}}$

Table 9. A^0 couplings to sfermion pairs with $c = g$

$\tilde{f}_{i\alpha}\tilde{f}^*_{i\beta}$	Γ
$\tilde{u}_{i\alpha}\tilde{u}^*_{i\beta}$	$\frac{m_{u_i}}{2M_W}\left(A_{u_i}\cot\beta+\mu\right)\delta_{\alpha\neq\beta}$
$\tilde{d}_{i\alpha}\tilde{d}^*_{i\beta}$	$\frac{m_{d_i}}{2M_W}\left(A_{d_i}\tan\beta+\mu\right)\delta_{\alpha\neq\beta}$
$\tilde{l}_{i\alpha}\tilde{l}^*_{i\beta}$	$\frac{m_{l_i}}{2M_W}\left(A_{e_i}\tan\beta+\mu\right)\delta_{\alpha\neq\beta}$

neutralino rules are related to the unprimed ones via

$$N'_{i1} = N_{i1}\cos\theta_\mathrm{W} + N_{i2}\sin\theta_\mathrm{W}\,, \tag{D.1a}$$
$$N'_{i2} = N_{i2}\cos\theta_\mathrm{W} - N_{i1}\sin\theta_\mathrm{W}\,, \tag{D.1b}$$
$$N'_{i3} = N_{i3}\,, \tag{D.1c}$$
$$N'_{i4} = N_{i4}\,. \tag{D.1d}$$

References

1. S. Gieseke, A. Ribon, M.H. Seymour, P. Stephens, B. Webber, JHEP **0402**, 005 (2004) [arXiv:hep-ph/0311208]
2. S. Gieseke et al., arXiv:hep-ph/0609306
3. G. Corcella et al., arXiv:hep-ph/0210213
4. G. Corcella et al., JHEP **0101**, 010 (2001) [arXiv:hep-ph/0011363]
5. S. Moretti, K. Odagiri, P. Richardson, M.H. Seymour, B.R. Webber, JHEP **0204**, 028 (2002) [arXiv:hep-ph/0204123]
6. F. Maltoni, T. Stelzer, JHEP **0302**, 027 (2003) [arXiv:hep-ph/0208156]
7. A. Pukhov et al., arXiv:hep-ph/9908288
8. T. Gleisberg, S. Hoche, F. Krauss, A. Schalicke, S. Schumann, J.C. Winter, JHEP **0402**, 056 (2004) [arXiv:hep-ph/0311263]
9. M. Moretti, T. Ohl, J. Reuter, arXiv:hep-ph/0102195
10. W. Kilian, WHIZARD 1.0: A generic Monte Carlo integration and event generation package for multi-particle processes. Manual
11. P. Skands et al., JHEP **0407**, 036 (2004) [arXiv:hep-ph/0311123]
12. L. Randall, R. Sundrum, Phys. Rev. Lett. **83**, 3370 (1999) [arXiv:hep-ph/9905221]
13. P. Richardson, JHEP **0111**, 029 (2001) [arXiv:hep-ph/0110108]
14. J.C. Collins, Nucl. Phys. B **304**, 794 (1988)
15. I.G. Knowles, Comput. Phys. Commun. **58**, 271 (1990)
16. H. Murayama, I. Watanabe, K. Hagiwara, KEK-91-11
17. B.C. Allanach, K. Odagiri, M.J. Palmer, M.A. Parker, A. Sabetfakhri, B.R. Webber, JHEP **0212**, 039 (2002) [arXiv:hep-ph/0211205]
18. B.C. Allanach, K. Odagiri, M.A. Parker, B.R. Webber, JHEP **0009**, 019 (2000) [arXiv:hep-ph/0006114]
19. B.C. Allanach et al., In: N. Graf (Ed.), Proc. APS/DPF/DPB Summer Study on the Future of Particle Physics (Snowmass 2001), Snowmass, Colorado, 30 June–21 July 2001, pp. P125 [arXiv:hep-ph/0202233]
20. B.C. Allanach, Comput. Phys. Commun. **143**, 305 (2002) [arXiv:hep-ph/0104145]
21. B.C. Allanach, C.G. Lester, M.A. Parker, B.R. Webber, JHEP **0009**, 004 (2000) [arXiv:hep-ph/0007009]
22. T. Han, J.D. Lykken, R.J. Zhang, Phys. Rev. D **59**, 105 006 (1999) [arXiv:hep-ph/9811350]
23. S.Y. Choi, K. Hagiwara, Y.G. Kim, K. Mawatari, P.M. Zerwas, arXiv:hep-ph/0612237
24. S. Jadach, Z. Was, R. Decker, J.H. Kuhn, Comput. Phys. Commun. **76**, 361 (1993)
25. B.K. Bullock, K. Hagiwara, A.D. Martin, Phys. Rev. Lett. **67**, 3055 (1991)
26. J.M. Smillie, B.R. Webber, JHEP **0510**, 069 (2005) [arXiv:hep-ph/0507170]
27. R. Kleiss, W.J. Stirling, Nucl. Phys. B **262**, 235 (1985)
28. H.E. Haber, arXiv:hep-ph/9405376
29. L. Lonnblad, Nucl. Instrum. Methods A **559**, 246 (2006)